

Anti-corrosive propensity of naturally occurring aldehydes and 1-(3-aminopropyl)imidazole condensed Schiff bases: Comparison on the effect of extended conjugation over electron donating substituents



Sanjoy Satpati^{a,b}, Aditya Suhasaria^a, Subhas Ghosal^a, Utpal Adhikari^a, Priyabrata Banerjee^{c,d}, Sukalpa Dey^e, Dipankar Sukul^{a,*}

^a Department of Chemistry, National Institute of Technology, Durgapur 713 209, India

^b Department of Chemistry, Government General Degree College, Tehatta, Nadia 741 160, India

^c Surface Engineering and Tribology Group, CSIR-Central Mechanical Engineering Research Institute, Durgapur 713209, India

^d Academy of Scientific and Innovative Research (AcSIR), AcSIR Headquarters CSIR-HRDC Campus, Sector-19, Kaila Nehru Nagar, Ghaziabad 201002, India

^e Department of Basic Science and Humanities, Dr. B. C. Roy Engineering College, Durgapur 713 206, India

ARTICLE INFO

Article history:

Received 25 May 2022

Revised 4 July 2022

Accepted 6 July 2022

Available online 8 July 2022

Keywords:

Mild steel

Schiff base

Corrosion inhibitor

DFTB+

Irreversibility test

ABSTRACT

Schiff bases prepared by condensation of 1-(3-aminopropyl)imidazole and three different naturally occurring aldehydes, namely salicylaldehyde, vanillin and cinnamaldehyde (ISSB, IVSB and ICSB, respectively) are tested as corrosion inhibitors for mild steel in 1 M HCl. Comparative effects of extended conjugation and +R effect bestowed by the electron donating group are explored towards the extent of corrosion protection of mild steel. ICSB, having extended conjugation, stands out to be the most efficient one. At 1 mM concentration, it imparts nearly 99% inhibition efficiency at 40 °C after 48 h of exposure of mild steel in 1 M HCl. DFTB+ study reveals the active centers of inhibitor molecules responsible for bi-directional electron transfer with metal surface. Irreversibility test with ICSB layer formed after exposure in 1 M HCl for 24 h having 1 mM ICSB, provides 78% inhibition efficiency to mild steel when exposed to the uninhibited 1 M HCl for 3 h. From detailed temperature dependence study, thermodynamics and kinetic parameters are obtained, which are instrumental to ascertain the nature of adsorption of the studied inhibitors.

© 2022 Elsevier B.V. All rights reserved.

1. Introduction

A variety of Schiff bases have been investigated for their potential anti-corrosive activities both for ferrous and non-ferrous metals and alloys in recent past [1–14]. Schiff bases possess several characteristics conducive for corrosion mitigation. However, in many cases the reported inhibition efficiencies are not very high. In some instances, the inhibitory effect does not last long, particularly at elevated temperature. These shortcomings are associated with the insolubility of Schiff bases, as well as instability of the inhibitor layer in highly acidic medium under prolonged exposure or at higher temperature. In addition, report on the irreversibility test for corrosion inhibitors, *i.e.*, how long the inhibitor layer can sustain in the aggressive uninhibited acid solution, is really scarce [15]. This is an important aspect in regard to applicability of inhibitors in real situation. Most of the works involving Schiff bases as corrosion inhibitors focus on the effect of multiple imine bonds,

presence of electron donating/withdrawing groups, aromatic moieties, heteroatoms, aliphatic chain length etc. [1–14]. Some studies have pointed out better performance of the Schiff bases having extended conjugation, which results into higher electron density on the imine group [3,16–18]. In the present work, we intend to present a comparative study between the effect of extended conjugation and that of electron donating substituents. For this, we have used structurally comparable inhibitor molecules and took mild steel as the test material and 1 M aqueous HCl as the corrosive medium. Mild steel is one of the most widely used structural materials because of its strength, malleability, ductility, weldability, machinability, and most-importantly cost effectiveness [19]. As it is very prone towards corrosion, protecting mild steel, particularly from mineral acid environment like HCl is still a challenge [19]. There are diversified uses of mineral acids like HCl. These include chemical processing, pickling, acid de-scaling, oil-well acidifying processes and many others [20]. During these processes, as well as during transportation and storage of acid, application of suitable corrosion retardant is a pre-requisite.

* Corresponding author.

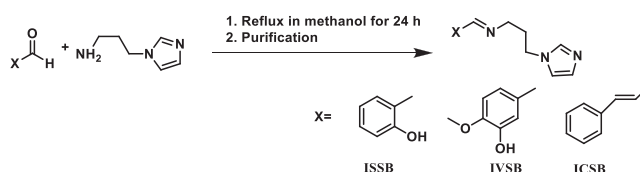
E-mail address: dipankar.sukul@ch.nitdgp.ac.in (D. Sukul).

Table 1
Molecular name and structure of studied Schiff bases.

Molecular name	Molecular structure	MW	Abbreviation
2-(((3-(1H-imidazol-1-yl)propyl)imino)methyl)phenol		229.3	ISSB
4-(((3-(1H-imidazol-1-yl)propyl)imino)methyl)-2-methoxyphenol		259.3	IVSB
(1E,2E)-N-(3-(1H-imidazol-1-yl)propyl)-3-phenylprop-2-en-1-imine		239.3	ICSB

Our group has reported the corrosion inhibition efficacy of Schiff bases composed of cinnamaldehyde or vanillin with different amines towards mild steel in aqueous HCl [3,8]. Approaching differently in the present work, three Schiff bases are prepared condensing three naturally available aldehydes, namely salicylaldehyde, vanillin and cinnamaldehyde separately with 1-(3-aminopropyl)imidazole. Structures of the Schiff bases and their nomenclatures are given in Table 1. 1-(3-aminopropyl)imidazole is an important imidazole derivative with many potential applications in material science, particularly when grafted or functionalized with other polymers [21,22]. The imidazole and aldehyde moieties along with the imine bond should be involved in adsorption of the inhibitors on metal surface through the heteroatoms and the π -electrons, while the propyl group is expected to impart hydrophobicity towards the adsorbed layer. Comparing ISSB and IVSB, the later contains an additional electron donating methoxy group. Such electron donating group enhances the possibility of electron transfer to the metal, and thus the corrosion inhibition efficiency [12,13,23,24]. ICSB, on the other hand, possesses a C=C, leading to an extended conjugation between the imine bond and the aromatic group. The choice of inhibitors, which are structurally comparable, has allowed to investigate whether the extended conjugation or the electron donating group exhibits better corrosion inhibitory performance towards mild steel in 1 M aqueous HCl. Another important aspect of corrosion inhibitor is its bio-compatibility and environmental benign characteristics. The preparation method should also be environment friendly. The aldehydes used in the present work are naturally available. Further, the synthesis process requires only ethanol as the solvent. Hence it may be concluded that there should not be any adverse effect to the environment either during the synthesis of the Schiff bases, nor by using those molecules. Different electrochemical methods (Tafel extrapolation and electrochemical impedance spectroscopy) and gravimetric experimentation are carried out. From these studies, the adsorption and kinetic parameters are calculated. These experimental results enable to elucidate the mechanism of inhibitor adsorption on mild steel in aqueous HCl and subsequent corrosion inhibition. From the density functional theory

(DFT), different intrinsic molecular parameters of the studied Schiff bases are evaluated. These parameters are used to correlate the reactivity of the corrosion inhibitors to their molecular structures. Interaction of the Schiff bases with mild steel surface is investigated in electronic details through density functional based tight binding approach (DFTB+) introducing Fe (1 1 0) surface of dimension $7 \times 7 \times 4$.

**Scheme 1.** General scheme for preparation of the inhibitor molecules.

2. Experimental

2.1. Preparation and characterization of inhibitors

A general scheme for preparation of the inhibitor molecules is depicted in Scheme 1. Detail of the preparation procedure is also provided as follows:

ISSB: 1.2212 g (10 mM) of salicylaldehyde (Sigma-Aldrich, 98%) was taken in 30 ml methanol and to this solution 1.2517 g (10 mM) 1-(3-aminopropyl)imidazole (Sigma-Aldrich, 97%) was added drop wise with constant stirring and the mixture refluxed for 24 h. The solvent was removed using rotary evaporator to give a yellow oil, which on standing for overnight yielded yellow crystals of ISSB (yield ~85%).

IVSB: To a solution of 1.5215 g (10 mM) of vanillin ((Sigma-Aldrich, 99%) in 30 ml methanol, 1.2517 g (10 mM) 1-(3-aminopropyl)imidazole was added drop wise with constant stirring and the mixture refluxed for 24 h to give yellowish color solution. Solvent was removed under reduced pressure. The product was taken in chloroform, washed with water for several times. CHCl_3 layer was dried over anhydrous sodium sulfate. Removal of CHCl_3 under reduced pressure gave IVSB (reddish oily liquid, yield ~81%).

ICSB: To a solution of 1.3216 g (10 mM) of trans-cinnamaldehyde (Sigma-Aldrich, 99%) in 30 ml methanol, 1.2517 g (10 mM) 1-(3-aminopropyl)imidazole was added drop wise with constant stirring. The mixture was refluxed for 24 h to give reddish-yellowish colored solution. Solvent was removed under reduced pressure. The product was taken in chloroform, washed with water for several times. CHCl_3 layer was dried over anhydrous sodium sulfate. Removal of CHCl_3 under reduced pressure resulted ICSB (reddish oily liquid, yield ~82%).

Characterization of synthesized inhibitors:

$^1\text{H NMR}$: ISSB: δ ppm 13.117 (s, 1H, -O-H), 8.311 (s, 1H, H^c), 7.451 (s, 1H, H^i), 7.335–7.300 (dt, 1H, H^c), 7.230–7.226 (dd, 1H, H^b), centered at 7.068 (1H, H^j), 6.968–6.947 (dd, 1H, H^a), centered at

6.911 (1H, H^k), 6.886–6.865 (dd, 1H, H^d), 4.078–4.044 (t, 2H, H^h), 3.559–3.524 (t, 2H, H^f), 2.217–2.150 (quintet, 2H, H^g) (Fig. S1 in SI)

IVSB: δ ppm 7.979 (s, 1H, H^d), 7.408 (s, 1H, H^h), 7.282–7.277 (d, 1H, H^c), centered at 6.960 (d, 1H, Hⁱ), centered at 6.932 (d, 1H, H^j), centered at 6.843 (s, 1H, H^a), 6.808–6.788 (d, 1H, H^b), 3.947–3.912 (t, 2H, H^g), 3.725 (s, 3H, –OCH₃ group), 3.419–3.386 (t, 2H, H^e), 2.080–2.012 (quintet, 2H, H^f) (Fig. S1 in SI)

ICSB: δ ppm 7.972–7.951 (d, 1H, H^h), 7.464–7.289 (6H, H^a, H^b, H^c, H^d, H^e & H^f), centered at 7.022–6.917 (2H, H^m & Hⁿ), 6.894–6.821 (m, 2H, H^f & H^g), 4.023–3.987 (t, 2H, H^k), 3.445–3.410 (t, 2H, Hⁱ), 2.127–2.065 (quintet, 2H, H^j) (Fig. S1 in SI)

ESI-Mass: Appearance of strong molecular ion peak [L-H]⁺ at m/z 230.1285 (100%), 260.1397 (100%), 240.1492 (75%) confirms the formation of ISSB, IVSB and ICSB, respectively. Appearance of peaks at 354.1959 [L+3K-2H, 100%], 258.1956 [L+H₂O+H, 75%] also confirm formation of ICSB. Appearance of ion peaks at higher than 354.1959 suggests the possibility of some trace amount of impurities in the sample (Fig. S2 in SI).

FTIR: Appearance of a define peak in the range 1631–1637 cm⁻¹ in corresponding FTIR spectra of the synthesized Schiff bases confirms the formation of imine bond due to condensation of aldehyde and the amine groups [3,8]. Bands in the region 1570–1590 cm⁻¹ are assigned to the stretching vibration of aromatic C=N of imidazole ring, whereas those in the range 1510–1450 cm⁻¹ are due to various types of C=C vibrations (Fig. S3 in SI).

2.2. Preparation of metal surface for corrosion test

Mild steel coupons of dimension 2.5 × 2.5 × 0.1 cm³ with average elemental composition (wt%) of 0.22 C, 0.31 Si, 0.60 Mn, 0.04 P, 0.06 S and the rest iron, are used in this study. Surface of the coupons are abraded with different grade SiC paper with grits ranging from 400 to 1200. This is followed by washing with liquid detergent, running water, distilled water and finally with acetone. Coupons are polished using velvet cloth before use [3,8].

2.3. Electrochemical measurements

A potentiostat with embedded frequency response analyzer (model: GILL AC, UK) is employed for electrochemical measurement. Three electrode system with mild steel coupon (exposed area 0.5 cm² in 250 mL 1 M aqueous HCl) as the working electrode, saturated calomel electrode (SCE) as the reference and Pt mesh electrode as the auxiliary one are used for electrochemical measurement. An exposure for 40 min to 1 M HCl provides stable open circuit potential (OCP) for the mild steel coupons. Thereafter, potential is scanned within a range of ± 250 mV from OCP with a scan rate of 1 mV s⁻¹ which yielded the polarization curves. Curves are fitted following Tafel extrapolation method to obtain various corrosion parameters, including the corrosion current density (*i*_{corr}). Inhibition efficiency is calculated from the Eq. (1)

$$\eta_p(\%) = \frac{i_{\text{corr}} - i_{\text{corr(inh)}}}{i_{\text{corr}}} \times 100 \quad (1)$$

where, *i*_{corr} stands for the corrosion current density in the uninhibited solution, and *i*_{corr(inh)} is for that in the presence of inhibitor.

Electrochemical impedance experiment is done applying an AC voltage of ± 10 mV with respect to the OCP and with a varied frequency within the range of 100 kHz to 0.01 Hz. By fitting the Nyquist plots with suitable equivalent circuit model, values of the polarization resistance with and without the inhibitor (*R*_p and *R*_p⁰, respectively) are obtained and the inhibition efficiency is calculated as per Eq. (2):

$$\eta_z(\%) = \frac{R_p - R_p^0}{R_p} \times 100 \quad (2)$$

2.4. Weight loss method

With properly polished test coupons weight loss measurement is done in 1 M HCl (350 mL) for 6–96 h and within a temperature range of 20–60 °C [3,8]. Eq. (3) corresponds to the inhibition efficiency (η_w) from the values of weight loss in the absence and presence of inhibitor (*W*₀ and *W*, respectively).

$$\eta_w(\%) = \frac{W_0 - W}{W_0} \times 100 \quad (3)$$

After proper cleaning (described in Section 2.2), the test coupons are dried in vacuum desiccator. Taking the initial weight, the dried coupons are immersed in 350 mL of aqueous HCl (1 M) in the absence and presence of inhibitors. After different exposure time, the coupons are taken out, and washed under running water using a bristled brush. This is followed by washing with distilled water and acetone and finally dried in a vacuum desiccator before taking their final weight. During long exposure, the volume of the solution is maintained by adding the requisite amount of distilled water when required [9].

Data reported on electrochemical and gravimetric methods is the mean of three different sets of experimentation.

2.5. Surface analysis

SEM images of the corroded metal surface in the presence and absence of inhibitors are taken by Hitachi S-3000 N microscope equipped with an EDAX attachment. The latter is used for elemental analysis of metal surface.

2.6. Computational details

Density functional theory (DFT) calculation is done with DMol³ computational package in Biovia Materials studio 2020 applying B3LYP functional with both DND and DNP basis sets. Effect of solvent water is introduced through COSMO model [25]. Convergence tolerance of energy is set at 10⁻⁶ Ha, whereas the SCF tolerance at 10⁻⁶. From the energies of the highest occupied molecular orbital (HOMO) and lowest unoccupied molecular orbital (LUMO), we calculate the absolute electronegativity (χ , signifies the electron attracting ability of a chemical system), global hardness (η , a parameter signifying the resistance of a chemical system towards charge transfer), and global softness (σ , an indicator of the susceptibility or easiness towards charge transfer) following the Eqs. (4)–(6) [26–30]

$$\chi = -(E_{\text{HOMO}} + E_{\text{LUMO}})/2 \quad (4)$$

$$\eta = -(E_{\text{HOMO}} - E_{\text{LUMO}})/2 \quad (5)$$

$$\sigma = 1/\eta \quad (6)$$

The fraction of total electron density transferred from inhibitor to the metal (ΔN_{110}) is calculated using following Eq. (7) :

$$\Delta N_{110} = \frac{(\phi_{\text{Fe}} - \chi_{\text{inh}})}{2(\eta_{\text{Fe}} + \eta_{\text{inh}})} \quad (7)$$

Here, ϕ_{Fe} , the work function of Fe (1 1 0) surface, is taken as 4.82 eV [31,32]. For Fe, (1 1 0) surface has maximum stability and highest packing density. As a result, extent of interaction of organic inhibitor molecules with this Fe surface is supposed to be higher than with the other surfaces [33]. The global hardness of Fe (η_{Fe}) is taken as zero, as HOMO and LUMO overlap for the metal [31–33].

2.7. Calculation of Fukui indices

Fukui indices of atom which parameterize the local reactivity of atoms in a molecule towards attack by a nucleophilic and electrophilic (f_k^+ and f_k^- , respectively), is calculated with the help of the DMol³ module in Biovia Materials studio 2020.

Positive and negative Fukui indices are calculated by the Eqs. (8) and (9):

$$f_k^+ = q_k(N+1) - q_k(N) \quad (8)$$

$$f_k^- = q_k(N) - q_k(N-1) \quad (9)$$

where, $q_k(N+1)$, $q_k(N)$ and $q_k(N-1)$ describe the gross atomic charge of the atom k in $(N+1)$, N and $(N-1)$ electron systems, respectively [34].

2.8. Molecular dynamics simulation

On a slab of Fe (1 1 0) plane comprising $20 \times 20 \times 10$ (length \times breadth \times depth) numbers of Fe atoms, a vacuum slab is put on the top, so that the overall dimension of the simulation box becomes $49.647 \times 49.647 \times 98.241$ Å with periodic boundary condition. One inhibitor molecule, 500 number of water molecules, 10 number each of H_3O^+ and Cl^- ions are annealed within the box using adsorption locator module of Materials studio fixing the coordinates of all the Fe atoms. It is followed by MD simulation employing COMPASSIII force field for 100 ps with a time step of 1.0 fs at an average temperature of 25 °C considering canonical ensemble (NVT) and Berendsen thermostatic conditions (forcite module of Materials Studio 2020). Interaction energy ($E_{interaction}$) between the inhibitor molecule and Fe surface is calculated as,

$$E_{interaction} = E_{total} - (E_{surface+H_2O+H_3O^+Cl^-} + E_{inhibitor}) \quad (10)$$

where, E_{total} represents total energy of the simulated system, $E_{surface+H_2O+H_3O^+Cl^-}$ and $E_{inhibitor}$ correspond to energy of the surface including the electrolytic solution and energy of the free inhibitor, respectively [3,5,8].

2.9. DFTB+ calculation

A slab of Fe (1 1 0) planes with $7 \times 7 \times 4$ number of Fe atoms is constructed and along with a vacuum slab the overall lattice dimension with period boundary condition becomes $17.376 \times 17.376 \times 31.080$ Å. Introducing one inhibitor molecule into the bounding box, MD simulation with COMPASSIII force field is carried out applying all the same parameters as described in Section 2.8. Output of MD simulation is now subjected to DFTB+ calculation with dispersion correction after unfixing the coordinates of all the Fe atoms at the upper two layers (Material studio 2020) [35,36]. This allows unconstrained interaction with Fe atoms present in the top two layers with the inhibitor molecule. Convergence tolerance of energy was fixed at $0.02 \text{ kcal mol}^{-1}$, while that of displacement was 0.001 Å. SCC tolerance was set at 10^{-8} with thermal smearing and mixing parameter fixed at 0.005 Ha (Methfessel-Paxton smearing distribution function) and 0.2 (Broyden mixing scheme), respectively. Trans3d Slater-Koster library function with Divide and conquer eigensolver was selected for the calculation. k-point set was selected to be gamma ($1 \times 1 \times 1$).

3. Result and discussion

3.1. Variation of open circuit potential

Following Fig. S4 in SI, it is observed that the OCP values measured after immersion in aqueous HCl for 40 min in presence

of different inhibitor concentrations become almost constant with time and are within a narrow range of ± 15 mV. This shows comparable homogeneity regarding chemical property and surface morphology of the mild steel specimens, and also confirms the attainment of steady state in terms of surface reactions at the metal solution interface [37,38]. OCP does not change in any definite direction (cathodic or anodic) with inhibitor concentration. It suggests blocking of the reaction sites on metal surface by inhibitor molecules, and thereby affecting both the cathodic and anodic interfacial reactions [39].

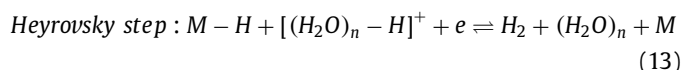
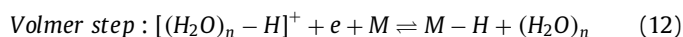
3.2. Potentiodynamic polarization

Fig. 1 illustrates how the potentiodynamic polarization plots of mild steel in 1 M HCl vary for different concentrations of the Schiff bases. The relevant corrosion parameters are shown in Table 2. It is observed that the Schiff bases drag the corrosion potential towards more negative values, effect being more pronounced at higher concentration. However, the change in potential is not so drastic to level the Schiff bases exclusively as cathodic inhibitors. In addition, the cathodic and anodic currents decrease for the whole potential range with increase in inhibitor concentration, the trend is being more prominent for the cathodic one. From these observations it is inferred that the Schiff bases are acting as mixed type inhibitors, with a relatively higher propensity to hinder the cathodic hydrogen evolution reaction [8,9,40]. Organic corrosion inhibitors are mostly of adsorption type, interacting with the metal surface through either chemisorption mode (electron transfer from the heteroatoms present or the π -electrons) or electrostatic means (positively charged molecule in acidic medium interacting with the metal surface adsorbed with Cl^- ions) [41].

These surface adsorbed non-conducting inhibitor layer interferes with the rate of cathodic and anodic processes. Table 2 reveals decrease in the cathodic and anodic Tafel slopes with increase in the inhibitor concentration. This is associated to decrease in the exchange current density values of the electrode reactions [42,43]. For example, applying the Tafel equation for the cathodic hydrogen evolution reaction (Eq. (11)), where η_c is the cathodic overpotential [44], it is observed that the corresponding exchange current density ($i_{o,H+/H_2}$) decreases from a value of $5.1 \times 10^{-5} \text{ A cm}^{-2}$ for uninhibited sample to $2.6 \times 10^{-7} \text{ A cm}^{-2}$ in presence of 1 mM ICSB.

$$\eta_c = (E_{corr} - E_{H^+/H_2}^0) = b_c \log \left(\frac{i_{corr}}{i_{o,H^+/H_2}} \right) \quad (11)$$

In the anodic sites, presence of inhibitors increases the electron density, and thereby favors metal ion reduction. Some inhibitors may even form complexes with metal ions and blocks the anodic sites from further oxidation. These induces increased anodic polarization behavior. The presence of inhibitor molecules at the cathodic reaction sites results into cathodic polarization by hindering the rate of hydrogen evolution reaction [43,44]. The cathodic Tafel slope values are found within a range of -140 mV to -110 mV per decade. This illustrates that either of the surface adsorption of hydrogen atom (Volmer step, Eq. (12)) or the recombination of surface adsorbed hydrogen atom to form molecular hydrogen (Heyrovsky step, Eq. (13)) will be the rate determining step [45,46].



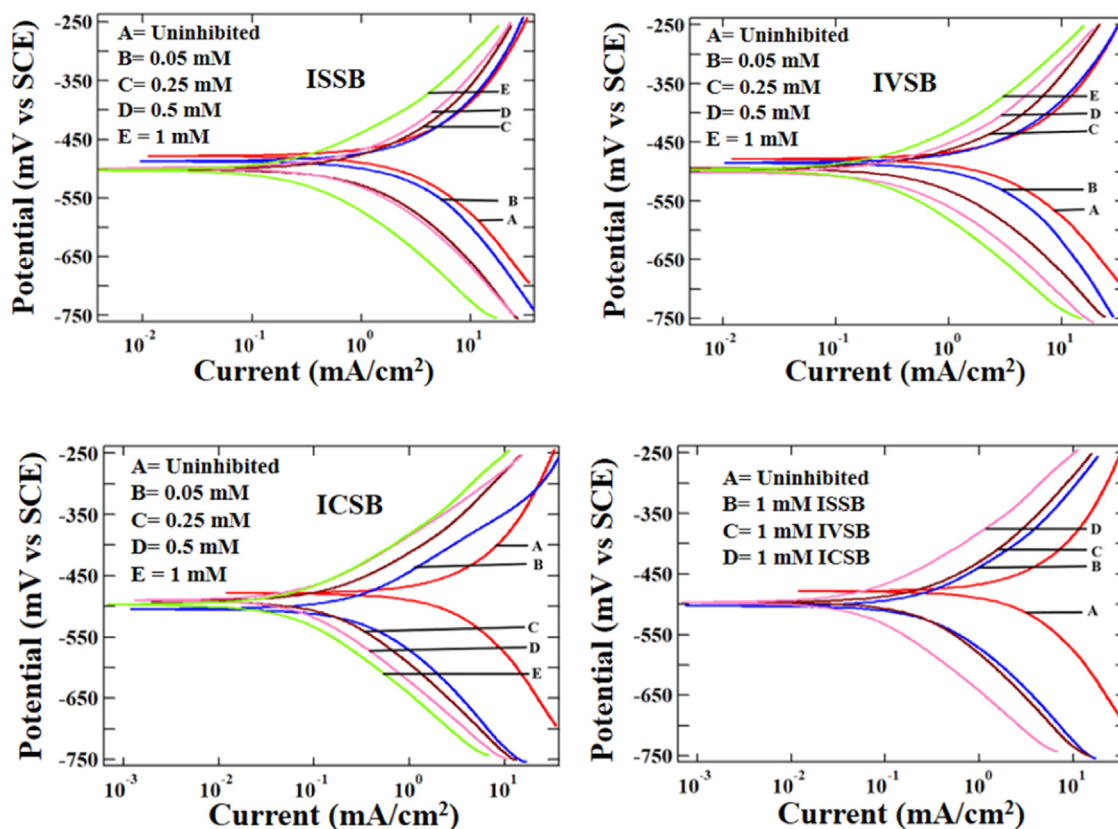


Fig. 1. Potentiodynamic polarization plots for mild steel in 1 M HCl at 30 °C with and without the Schiff bases.

Table 2

Corrosion parameters obtained from potentiodynamic polarization study at 30 °C.

Inhibitor	Conc. of inhibitor (mM)	$-E_{\text{corr}}$ (mV/SCE)	b_a (mVdec $^{-1}$)	$-b_c$ (mVdec $^{-1}$)	i_{corr} ($\mu\text{A cm}^{-2}$)	$\eta_p\%$
-	UNINHIBITED	478	131	145	2119	-
ISSB	0.01	480	123	132	1818	14.2
	0.05	487	120	129	1621	23.5
	0.10	492	113	128	1182	44.2
	0.25	499	109	125	769	63.7
	0.50	500	105	123	602	71.6
IVSB	1.00	504	102	121	247	88.3
	0.01	482	118	129	1797	15.2
	0.05	481	117	127	1388	34.5
	0.10	492	111	125	918	56.7
	0.25	495	106	123	622	70.6
ICSB	0.50	498	102	120	336	84.1
	1.00	498	99	117	195	90.8
	0.01	482	105	123	1127	46.8
	0.05	502	103	119	266	87.4
	0.10	497	100	117	209	90.1
	0.25	489	98	114	136	93.6
	0.50	491	95	111	74	96.5
	1.00	497	93	108	57	97.3

Net change in corrosion potential depends on the relative variation of anodic and cathodic polarization. In the present case, cathodic polarization exceeds the anodic polarization to some extent and thereby shifting the corrosion potential towards more negative, i.e., anodic side. Blocking of metal active sites results into substantial decrement in the corrosion current of mild steel in 1 M HCl, from around $2100 \mu\text{A cm}^{-2}$ in uninhibited solution to around $55 \mu\text{A cm}^{-2}$ in the presence 1 mM of ICSB. Inhibition efficiency following polarization experiment varies from 88% for ISSB to 90% for IVSB to 97% for ICSB at their 1 mM concentration level at 30 °C.

3.3. Electrochemical impedance spectroscopy (EIS)

EIS is nearly a non-destructive method to investigate any electrochemical system, as it is based on an AC perturbation of very small amplitude at the OCP [47]. The EIS reveals only one capacitive loop in the Nyquist plots of mild steel in 1 M HCl at all the inhibitor concentrations (Fig. 2). This reflects one time constant associated with the charge transfer reaction at the metal solution interface. This is further evidenced from the one negative slope in Bode impedance plots and one maximum in the corresponding Bode phase angle plots (Fig. S5 in SI). Accordingly, the EIS plots are fit-

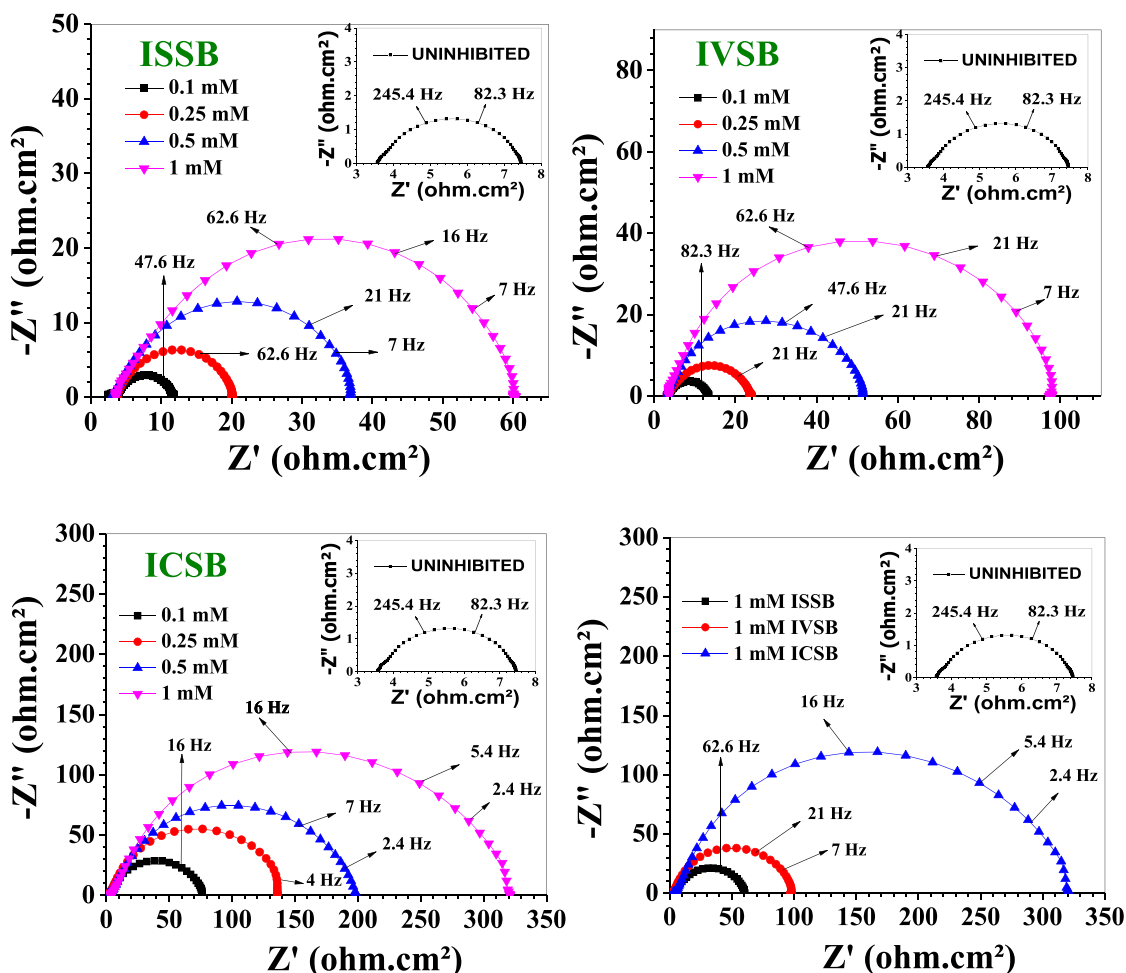


Fig. 2. Nyquist plots of mild steel in 1 M HCl with various inhibitor concentrations at 30 °C.

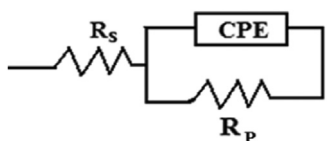


Fig. 3. Equivalent circuit used for fitting the impedance plots.

ted with an equivalent circuit as shown in Fig. 3, where CPE is the constant phase element, R_p being the polarization resistance (representing combined resistivity term which includes charge transfer resistance, resistance imparting by the adsorbed layers of corrosion inhibitors and corrosion products), while R_s is the solution resistance [48–53].

Use of CPE instead of capacitive element (C_{dl}) is to take care of the depressed semicircular nature of the Nyquist plots where the center of semicircles lies at a point under the real axis. This behavior is very common for corroded metal systems and is accounted for the surface heterogeneity [48–52]. In fact, surface heterogeneity results into distributed time-constant behavior, and the impedance response is described in terms of CPE [48–50]. Impedance of the CPE is given as:

$$Z_{CPE} = Q^{-1}(i\omega)^{-n} \quad (15)$$

where, Q and n are two parameters, using which one can recalculate the value of effective double layer capacitance, C_{dl} following

the Brug equation (Eq. (16)) [48–50].

$$C_{dl} = Q^{1/n} \left(\frac{R_s R_p}{R_s + R_p} \right)^{(1-n)/n} \quad (16)$$

This equation implies that when n is equal to 1 (which corresponds to a surface devoid of any surface heterogeneity), Q will assume the value of C_{dl} . All the calculated values after fitting the Nyquist plot with the equivalent circuit is summarized in Table 3. Applicability of the equivalent circuit and the goodness of fitting can be judged from the values of χ^2 , which is of the order of 10^{-4} . Diameter of the capacitive loops gradually increases with inhibitor concentrations, reflecting enhanced resistivity offered by the inhibitors with higher concentration towards charge transfer processes happening at the metal-electrolyte interface [48–53]. These charge transfer processes encompass both the cathodic hydrogen ion reduction and anodic Fe oxidation processes at the equilibrium condition. Thus, increase in R_p values with inhibitor concentration corresponds to the resistance to both the processes. Inhibition efficiency calculated in terms of R_p shows the similar trend in corrosion inhibition efficiency of the studied Schiff bases as observed in polarization experiment. The time constant, τ of the charge transfer process (which is calculated as $C_{dl} \times R_p$) increases with inhibitor concentration, and it reflects reduced dynamics of the system [53–56]. That the Schiff bases are diminishing the kinetics of charge transfer is also evident from the variation of frequency range where one attains the maximum value of the imaginary component of impedance in the Nyquist plots. Frequency

Table 3

Data obtained on fitting the Nyquist plots of mild steel in 1 M HCl with different inhibitor systems at 30 °C.

Inhibitor	Conc.(mM)	$R_s(\Omega \text{ cm}^2)$	$R_p(\Omega \text{ cm}^2)$	$Q(\mu\Omega^{-1} \text{ s}^n \text{ cm}^{-2})$	n	$C_{dl}(\mu\text{Fcm}^{-2})$	$\tau(\text{ms})$	$\eta_z\%$	$\chi^2 \times 10^4$
UNINHIBITED		3.7	3.8	789	0.84	228.1	0.87	-	0.91
	0.01	3.5	4.5	774	0.84	225.0	1.01	15.6	1.35
	0.05	3.3	6	614	0.84	173.3	1.04	36.7	9.8
	0.10	3.7	8	404	0.85	119.9	0.96	52.5	0.69
	0.25	3.7	16.6	235	0.85	65.4	1.08	77.1	0.76
	0.50	3.5	38.2	166	0.85	43.9	1.68	90.1	8.39
	1.00	3.7	56.9	154	0.85	40.8	2.32	93.3	9.9
IVSB	0.01	3.4	4.7	729	0.84	209.6	0.98	19.1	0.77
	0.05	3.5	6.2	597	0.84	169.2	1.05	38.7	9.4
	0.10	3.6	9.8	319	0.86	100.7	0.99	61.2	0.60
	0.25	3.5	20.3	182	0.86	53.5	1.09	81.3	0.88
	0.50	3.1	48.8	121	0.86	33.2	1.62	92.2	2.36
	1.00	3.1	96.3	81	0.88	26.04	2.51	96.1	3.54
	0.01	3.7	9.1	503	0.85	156.2	1.42	58.2	1.1
ICSB	0.05	3.1	59.7	118	0.86	32.2	1.92	93.6	2.29
	0.10	3.1	74.3	107	0.86	28.8	2.14	94.9	3.84
	0.25	3.2	141.4	77.5	0.88	24.9	3.52	97.3	1.53
	0.50	3.2	195.6	65.8	0.88	20.7	4.05	98.1	1.51
	1.00	3.2	314.6	60.7	0.87	16.9	5.32	98.8	3.15

range gradually decreases with inhibitor concentration and for ICSB the effect is most prominent (Table S1 in SI). Increase in inhibitor concentration leads to the increment in the phase angle value, as shown in the Bode phase plots (Fig. S5 in SI). This manifests reduced surface heterogeneity resulting from the adsorption of inhibitor molecules. Similar inference can be made by comparing the values of the parameter n for uninhibited and inhibited samples. In the presence of inhibitor layer, surface heterogeneity tends to reduce compared to that for the uninhibited sample and this is reflected into higher n value [48–53].

Increase in R_p with increasing inhibitor concentration is supplemented by the decrease in C_{dl} value. For the uninhibited solution, C_{dl} value is in the range of $230 \mu\text{F cm}^{-2}$. This is relatively higher than that for a plane electrode, which usually lies within a range of $5\text{--}50 \mu\text{F cm}^{-2}$ [57]. C_{dl} depends on the electrode surface area A , the double layer thickness d and the dielectric constant of interfacial solution ϵ , as per Eq. (17), where ϵ_0 is the vacuum permittivity.

$$C_{dl} = \frac{\epsilon_0 \epsilon A}{d} \quad (17)$$

Relatively high value C_{dl} in the uninhibited solution can be explained by the formation of porous oxide layer on the mild steel surface after exposure in acid solution, which enhances the effective surface area [57]. In the presence of inhibitor layer, C_{dl} gradually decreases. This may be due to a combined effect of several factors, like decrease in the effective surface area available for double layer formation, increase in the double layer thickness due to the presence of inhibitor layer, replacement of preadsorbed water molecules from metal surface by the organic inhibitor molecules which results into decreased ϵ value [58,59]. At the highest inhibitor concentration with ICSB showing maximum effectiveness among the three studied inhibitors, we can estimate the thickness of the inhibitor layer following Eq. (17) [49]. It requires some approximations, like formation of uniform inhibitor layer on the mild steel surface and displacement of all the pre-adsorbed water molecules from the surface. Ellipsometric and XPS measurement show the average thickness of corrosion inhibitor layer on metal surface in aqueous solution be to of the order of $10\text{--}30 \text{ \AA}$ [60,61]. To match the value, ϵ of the inhibitor layer should be within a range of $20\text{--}60$, which is rather high for an organic non-polar molecule [62]. This high value of dielectric constant only can be explained in-terms of retention of some adsorbed water molecules along with the inhibitor layer. This illustrates that organic inhibitor molecule can replace the pre-adsorbed water molecules from the metal surface only partially.

3.4. Weight loss measurement

3.4.1. Temperature effect

Table 4 summarizes the effect of temperature on the rate of corrosion of mild steel in the presence and absence of inhibitors and also on the corrosion inhibition efficacies of the studied Schiff bases. Rate of corrosion increases with temperature, reaffirming corrosion as an activation driven process. The inhibition efficiency initially increases with temperature, reaching maximum at $40 \text{ }^\circ\text{C}$ and thereafter decreases. As corrosion is a surface phenomenon, the inhibition efficiency obtained from weight loss method can be correlated with the degree of surface coverage offered by the inhibitors. Thus, the observation suggests adsorption of inhibitors is temperature dependent. At lower temperature range, the extent of adsorption increases with temperature, reflecting the requirement of overcoming a minimum energy barrier for adsorption. This is consistent with the characteristics of chemisorption, which is essentially an activation induced process. At higher temperature, corrosion inhibition decreases. This is consistent with the exothermic nature of adsorption process. However, thermal degradation of organic corrosion inhibitors in harsh acidic environment cannot be ruled out. Among the three Schiff bases, ICSB exhibits strongest adsorption propensity and temperature sustainability.

3.4.2. Effect of immersion time

At $30 \text{ }^\circ\text{C}$, all the three Schiff bases are tested for their anti-corrosion effectiveness for a period upto 96 h (Fig. 4, Table S2 in SI). Inhibitors at 1 mM concentration exert maximum corrosion mitigation power after 48 h of immersion in 1 M HCl. It corresponds to the optimum level of adsorption of inhibitors on mild steel surface. After 48 h, inhibition efficiency of ISSB shows a declining trend. This may be associated with desorption of the ISSB molecules from the metal surface or degradation of the molecular structure in the presence of high acidic environment. However, other two, i.e., IVSB and ICSB retain their structural integrity, and thereby inhibition efficiency upto 96 h. ICSB stands out to be an excellent inhibitor with 99% of corrosion inhibition efficiency at 1 mM concentration level for mild steel exposed to 1 M HCl for 48 h.

3.4.3. Reversibility test

Till now, the effectiveness of the bare inhibitor layer when exposed to the corrosive environment without any inhibitor has not been reported. This irreversibility performance of the adsorbed inhibitor layer is important from their application point of view.

Table 4
Corrosion rate of mild steel after immersion of 6 h in 1 M HCl in the presence and absence of Schiff bases at different temperatures.

Temp. (K)	Inhibitor conc. (mM)	Corrosion rate (mg cm ⁻² h ⁻¹) ^a			η_w (%)		
		ISSB	IVSB	ICSB	ISSB	IVSB	ICSB
293	0	1.890					
	0.01	1.677	1.593	0.828	11.3	15.7	56.2
	0.05	1.264	1.174	0.151	33.1	37.9	92
	0.10	0.977	0.803	0.130	48.3	57.5	93.1
	0.25	0.539	0.423	0.084	71.5	77.6	95.6
	0.50	0.316	0.204	0.064	83.3	89.2	96.6
	1.00	0.212	0.142	0.049	88.8	92.5	97.4
303	0	3.636					
	0.01	3.185	3.032	1.567	12.4	16.6	56.9
	0.05	2.371	2.225	0.269	34.8	38.8	92.6
	0.10	1.807	1.516	0.229	50.3	58.3	93.7
	0.25	0.956	0.785	0.138	73.7	78.4	96.2
	0.50	0.567	0.371	0.105	84.4	89.8	97.1
	1.00	0.367	0.247	0.076	89.9	93.2	97.9
313	0	6.600					
	0.01	5.669	5.405	2.772	14.1	18.1	58
	0.05	4.151	3.947	0.409	37.1	40.2	93.8
	0.10	3.181	2.666	0.343	51.8	59.6	94.8
	0.25	1.637	1.340	0.178	75.2	79.7	97.3
	0.50	0.865	0.594	0.132	86.9	91	98
	1.00	0.561	0.370	0.073	91.5	94.4	98.9
323	0	9.231					
	0.01	8.197	7.717	10.096	11.2	16.4	57.2
	0.05	6.065	5.714	7.520	34.3	38.1	93.1
	0.10	4.735	3.905	5.256	48.7	57.7	94.3
	0.25	2.6031	2.040	2.911	71.8	77.9	96.7
	0.50	1.357	0.997	1.594	85.3	89.2	97.5
	1.00	1.071	0.674	1.178	88.4	92.7	98.5
333	0	11.552					
	0.01	10.524	3.951	0.312	8.9	12.6	53.6
	0.05	7.948	0.637	0.448	31.2	34.9	90.6
	0.10	6.377	0.526	0.679	44.8	54.5	91.9
	0.25	3.708	0.305	0.805	67.9	74.8	94.4
	0.50	2.253	0.231	0.838	80.5	86.2	95.1
	1.00	1.871	0.138	0.089	83.8	89.8	96.4

(* Within a maximum range of $\pm 5\%$)

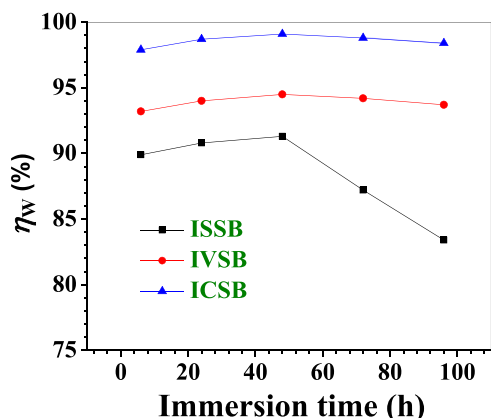


Fig. 4. Variation of the inhibition efficiency at 1 mM inhibitor concentration against immersion time at 30 °C.

Very scanty of literatures have highlighted this issue, but all in the presence of a supportive coating system [12]. Here, the mild steel coupons are first exposed to 1 mM ICSB solution in 1 M HCl for 24 h, so that the protective inhibitor coating is formed on the metal surface. These coupons are then exposed to 1 M HCl only at different time intervals. We then investigated the potentiality of these adsorbed layers in providing corrosion mitigation property in 1 M HCl without the presence of any inhibitor. Experimental data shows ICSB layer shows fair extent of irreversibility upto 3 h of exposure and we observe 78% inhibition efficiency. Extent of irre-

versibility gradually deteriorates and ICSB layer maintains 24–25% of inhibition efficiency upto 24 to 48 h.

3.5. Adsorption isotherm

From adsorption isotherm analysis, various adsorption parameters are evaluated. These parameters are instrumental in explaining the mechanism of adsorption of the studied Schiff bases on mild steel in aqueous HCl. For the studied system, Langmuir adsorption isotherm model (Eq. (18)) is found to be extremely good to fit the experimental data (C/θ vs C) with a wide range of concentration and at all temperatures (Figs 5 and S6 in SI). The near unity R^2 values validates the applicability of the Langmuir adsorption model (Table 5). Here, we have calculated degree of surface coverage, θ , from the Eq. (19). Some researchers recently have raised concerns over applicability of Eq. (19), as it is argued η_w and θ do not vary equally with inhibitor concentration [63].

$$\frac{C}{\theta} = \frac{1}{K_{ads}} + C \quad (18)$$

$$\theta = \eta_w(\%)/100 \quad (19)$$

If we consider η_w and θ be proportional to each other, then the proportionality constant will be reflected in slope values of the plots. Table 5 clearly shows that slopes for all the plots are very close to 1. This, on one side, validates the applicability of the Langmuir model, on the other side, it indicates the importance of considering the coverage of the active reaction sites and not the whole metal surface.

$$\Delta G_{ads}^0 = -RT \ln(55.55 K_{ads}) \quad (20)$$

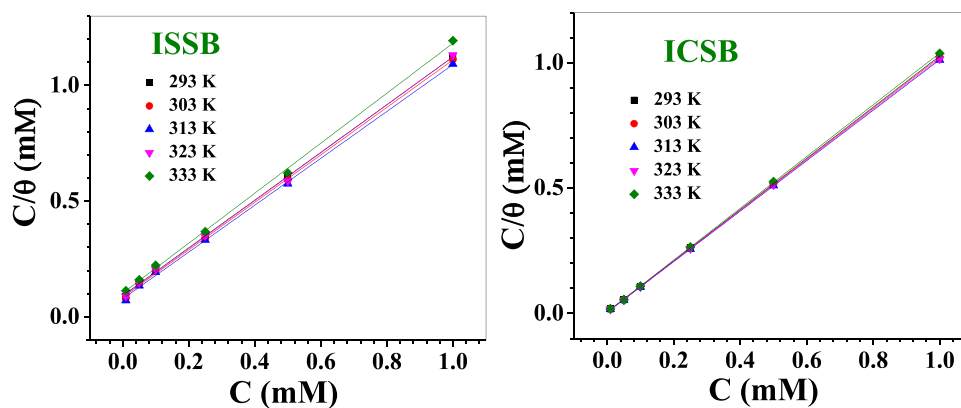


Fig. 5. Langmuir adsorption isotherms of mild steel in 1 M HCl containing ISSB and ICSB.

Table 5
Parameters obtained analysing the Langmuir adsorption isotherm.

Inhibitors	Temp (K)	R ²	Slope	Intercept (mmolar)	K _{ads} × 10 ⁻³ (molar ⁻¹)	- ΔG _{ads} ⁰ (kJ mol ⁻¹)
ISSB	293	0.999	1.0316	0.09203	10.87	32.42
	303	0.999	1.0262	0.08451	11.83	33.75
	313	0.999	1.0133	0.07734	12.93	35.09
	323	0.999	1.0352	0.08812	11.35	35.86
	333	0.999	1.0804	0.10248	9.76	36.55
IVSB	293	0.999	1.0093	0.06760	14.79	33.18
	303	0.999	1.0043	0.06518	15.34	34.40
	313	0.999	0.9949	0.06159	16.24	35.68
	323	0.999	1.0088	0.06649	15.04	36.62
	333	0.999	1.0301	0.07775	12.86	37.32
ICSB	293	0.999	1.0215	0.00571	175.13	39.20
	303	0.999	1.0164	0.00553	180.83	40.62
	313	0.999	1.0065	0.00532	187.97	42.06
	323	0.999	1.0105	0.00564	177.30	43.24
	333	0.999	1.0322	0.00649	154.08	44.19

Table 6
Standard enthalpy and entropy of adsorption for mild steel – Schiff base systems.

Method	Temp. (K)	ΔH _{ads} ⁰ (kJ mol ⁻¹)			ΔS _{ads} ⁰ (J K ⁻¹ mol ⁻¹)		
		ISSB	IVSB	ICSB	ISSB	IVSB	ICSB
Plots of ΔG _{ads} ⁰ vs. T	293-313	6.63	3.56	2.70	133	125	143
	313-333	-12.21	-10.13	-8.65	73	82	107
Plots of ΔG _{ads} ⁰ /T vs. 1/T	293-313	6.63	3.54	2.69	133	125	143
	313-333	-12.18	-10.06	-8.57	73	82	107

ΔG_{ads}⁰ values calculated from K_{ads} following Eq. (20), where 55.55 is taken as the concentration of water in mol L⁻¹. ΔG_{ads}⁰ values tend to become more negative with rise in temperature. ICSB, which exhibits the highest corrosion inhibition efficacy, has the maximum negative values of ΔG_{ads}⁰, and at temperatures higher than 20 °C, the values are well above 40 kJ mol⁻¹ (Table 5). For ISSB and IVSB, the ΔG_{ads}⁰ values are also not too far away from -40 kJ mol⁻¹. High negative values of ΔG_{ads}⁰ reaffirms strong adsorption of the three Schiff bases on the mild steel surface in aqueous HCl. Other adsorption parameters, ΔH_{ads}⁰ and ΔS_{ads}⁰, are calculated from two different methods, either plotting ΔG_{ads}⁰ vs. T or by plotting ΔG_{ads}⁰/T vs. 1/T (Eqs. (21), ((22)

$$\Delta G_{ads}^0 = \Delta H_{ads}^0 - T \Delta S_{ads}^0 \quad (21)$$

$$\Delta H_{ads}^0 = \left[\partial \left(\frac{\Delta G_{ads}^0}{T} \right) / \partial \left(\frac{1}{T} \right) \right]_p \quad (22)$$

(Figs. 6 and S7 in SI). Both methods yield comparable results (Table 6). Two different sets of values for ΔH_{ads}⁰ and ΔS_{ads}⁰ are obtained depending on temperature. At lower temperature range, ad-

sorption is endothermic, with relatively higher ΔS_{ads}⁰ values. But, at higher temperature range, it changes to exothermic nature with relatively lower values of ΔS_{ads}⁰. These observations can be explained if the desorption of pre-adsorbed water molecules is considered, at-least partially, during the adsorption of Schiff bases. Adsorption of water on metal or metal-organic framework is exothermic [64]. Thus, water desorption from metal surface is essentially endothermic, and at lower temperature range it out weights the exothermicity of Schiff base adsorption. The desorbed water molecules enhance the randomness of the system, producing higher ΔS_{ads}⁰ values. At elevated temperature, chemisorption of Schiff bases is energetically more favored and the heat released during this is more than the heat required for water desorption. ΔS_{ads}⁰ values are still seen to be positive and this indicates the adsorption of one Schiff base molecule is accompanied with the desorption of more than one water molecules from the metal surface.

3.6. Thermodynamic activation parameters

Kinetic parameters derived from plotting log(CR) vs. 1/T (Figs. 7 and S8 in SI) following the Arrhenius equation (Eq. (23)) and by

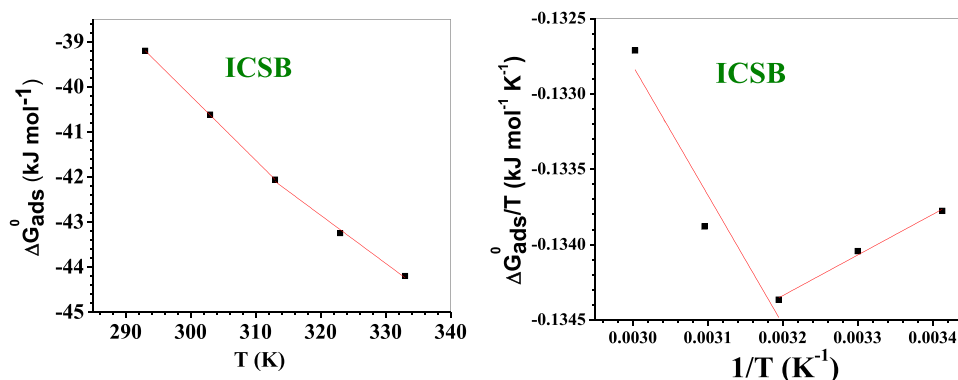


Fig. 6. Plot of ΔG_{ads}^0 vs. T (left) and $\frac{\Delta G_{ads}^0}{T}$ vs. $1/T$ (right).

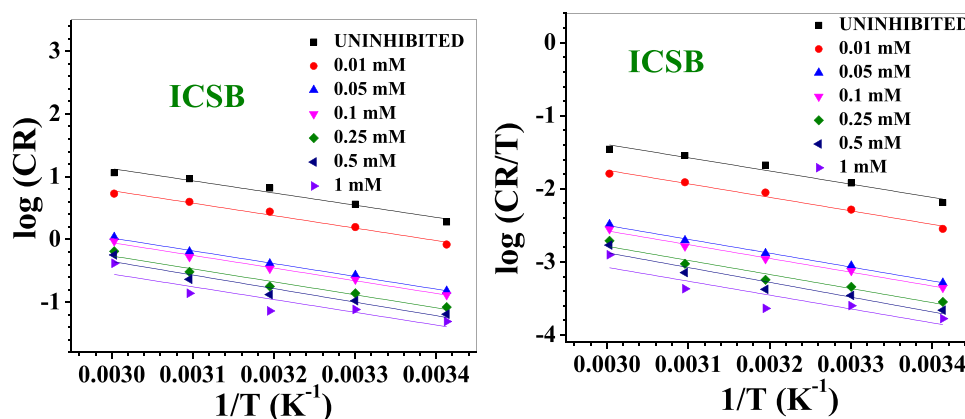


Fig. 7. Arrhenius and Eyring plots for corrosion of mild steel in 1 M HCl with ICSB.

Table 7

Activation parameters for corrosion of mild steel in 1 M HCl with and without inhibitors.

Inhibitors	Conc. (mM)	$\lambda \times 10^{-5}$ (mg cm ⁻² h ⁻¹)	E^* (kJ mol ⁻¹)	ΔH^* (kJ mol ⁻¹)	ΔS^* (J K ⁻¹ mol ⁻¹)	$E^* - \Delta H^*$ (kJ mol ⁻¹)
Uninhibited	0	90.28	37.19	34.60	-120.48	2.59
ISSB	0.01	97.12	37.70	35.11	-119.87	2.59
	0.05	70.94	37.65	35.06	-122.48	2.60
	0.10	74.35	38.43	35.84	-122.09	2.59
	0.25	61.87	39.54	36.93	-123.62	2.59
	0.50	28.24	38.97	36.38	-130.14	2.59
	1.00	136.95	43.94	41.35	-117.01	2.59
IVSB	0.01	94.43	37.76	35.16	-120.10	2.59
	0.05	76.41	38.00	35.41	-121.86	2.60
	0.10	59.77	38.35	35.75	-123.91	2.60
	0.25	42.93	39.16	36.57	-126.66	2.59
	0.50	49.22	41.40	38.80	-125.52	2.60
	1.00	49.40	42.41	39.82	-125.49	2.59
ICSB	0.01	53.91	38.01	35.42	-124.76	2.60
	0.05	13.43	38.97	36.37	-136.32	2.60
	0.10	10.19	38.68	36.09	-138.62	2.59
	0.25	8.34	39.47	36.88	-140.28	2.59
	0.50	13.33	41.33	38.74	-136.38	2.59
	1.00	3.55	38.94	36.34	-147.40	2.60

plotting $\log(CR/T)$ vs. $1/T$ (Figs. 7 and S8 in SI) as per the Eyring equation (Eq. (24)) are tabulated in Table 7.

$$\log CR = \log \lambda - \frac{E^*}{2.303 RT} \quad (23)$$

$$CR = \frac{RT}{N_A h} \exp\left(\frac{\Delta S^*}{R}\right) \exp\left(\frac{-\Delta H^*}{RT}\right) \quad (24)$$

As per the calculated data, the increased Schiff base concentration retards the rate of corrosion by increasing the activation energy with concomitant decrease in the pre-exponential frequency

factor (only exception is the 1 mM concentration of ISSB) Table 7). Following potentiodynamic polarization study, it is argued that the Schiff bases when present on metal surface affect the hydrogen evolution reaction more than the metal dissolution reaction. Thus, increase in the extent of adsorption of Schiff bases on metal surface not only provides an increasingly higher energy barrier towards the corrosion kinetics, but also results into decrease in the rate of effective encounter of H^+ on the inhibitor cladded metal surface. Variation of ΔH^* also supports the above explanation of enhanced energy barrier towards charge transfer process with the inhibitor concentration. ΔS^* values in the absence and presence of

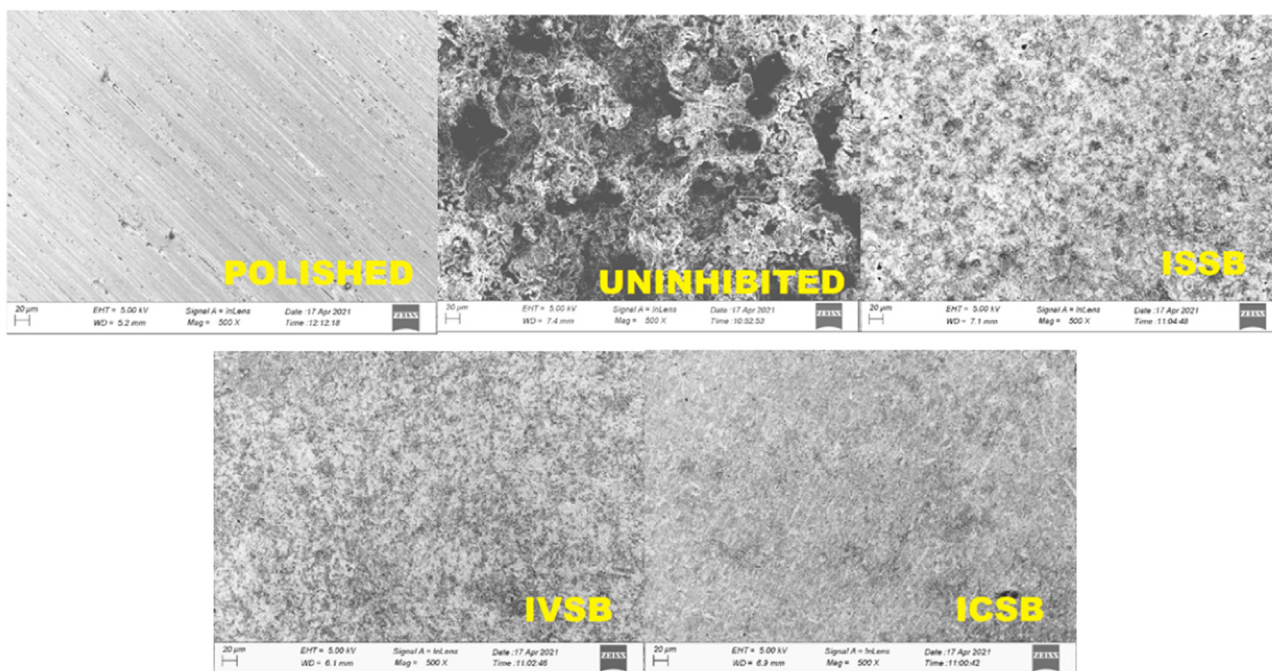


Fig. 8. SEM images of mild steel surface after immersing in 1 M HCl for 24 h without and with 1 mM inhibitors.

inhibitor are negative. This is indicative of more compact transition state in the rate determining step of the charge transfer process compared to reactants. The Volmer and Heyrovsky steps of hydrogen evolution reaction (Eqs. (12) and (13)) represent an increase in the orderness which explains the observed negative value of ΔS^* .

ΔS^* tends to be more negative with increase in inhibitor concentration, which is more pronounced for ICSB. This reflects in the presence of inhibitor layer, closer approach or interaction is required for the charge transfer process to happen, resulting a decrease in the randomness to a greater extent. Experimental data are consistent with the relation as per Eq. (25), which is applicable for a unimolecular gaseous reaction or a bimolecular reaction in

$$E^* - \Delta H^* = RT \quad (25)$$

solution. ($E^* - \Delta H^*$) values are nearly constant and the value (2.59–2.60 kJ mol⁻¹) is equal to RT , where T is taken as 313 K, i.e., the mean of the experimental temperatures.

3.7. Surface characterization

SEM images are indicative of the effectiveness of the studied Schiff bases as corrosion inhibitors. The order of inhibition efficiency as obtained experimentally is clearly manifested in the observed SEM images (Fig. 8). ICSB being the most effective corrosion inhibitor among the studied Schiff bases, results into the cleanest surface image, whereas in the presence of ISSB, relatively more pits and roughened areas are seen. Weight percentages of the elements present at the surface is analyzed by EDAX (Fig. S9 in SI, Table 8). O content at the surface of the uninhibited sample is very high, reflecting the formation of oxide layer on the metal surface. In the presence of inhibitors, surface O content decreases in the order of increased inhibition efficiency. In the presence of ICSB, weight percentages of elements are seen to be very close to those for the polished surface, exhibiting its highest capability among the three inhibitors in mitigating corrosion of mild steel against 1 M HCl.

3.8. DFT calculation

For all theoretical calculation, only the neutral forms of inhibitor molecules are considered. In a series of seminal works, Liu et al. have established that adsorption of azole molecules in their neutral state is much more probable than through protonated state [65,66]. In our previous works, we have also argued in the same line. Protonated inhibitor molecule may play its part during initial stage of adsorption through long range electrostatic interaction. But when a close distance of approach with the metal surface is achieved, it is the neutral form of the inhibitor which is more likely to interact with the metal surface [3,8,9]. The geometry optimized structures of the studied Schiff bases are shown in Fig. 9 along with electron distribution in their HOMO and LUMO energy levels. It is seen that the phenyl ring of the aldehyde moiety extended upto the imine linkage is aligned nearly perpendicularly with the imidazole ring. For IVSB and ICSB, electron distribution in HOMO and LUMO are very much identical, in both the cases these are distributed over the aldehyde moiety and the attached imine group. For ISSB, similar distribution is observed for the LUMO. For HOMO the electron distribution is quite different, it is extended over almost the whole molecular surface, i.e., including the imidazole ring. This indicates a possible difference in interaction pattern for ISSB with the metal surface with those for IVSB or ICSB. Energies of the frontier molecular orbitals along with other intrinsic molecular parameters are tabulated in Tables 9 and S3 in SI.

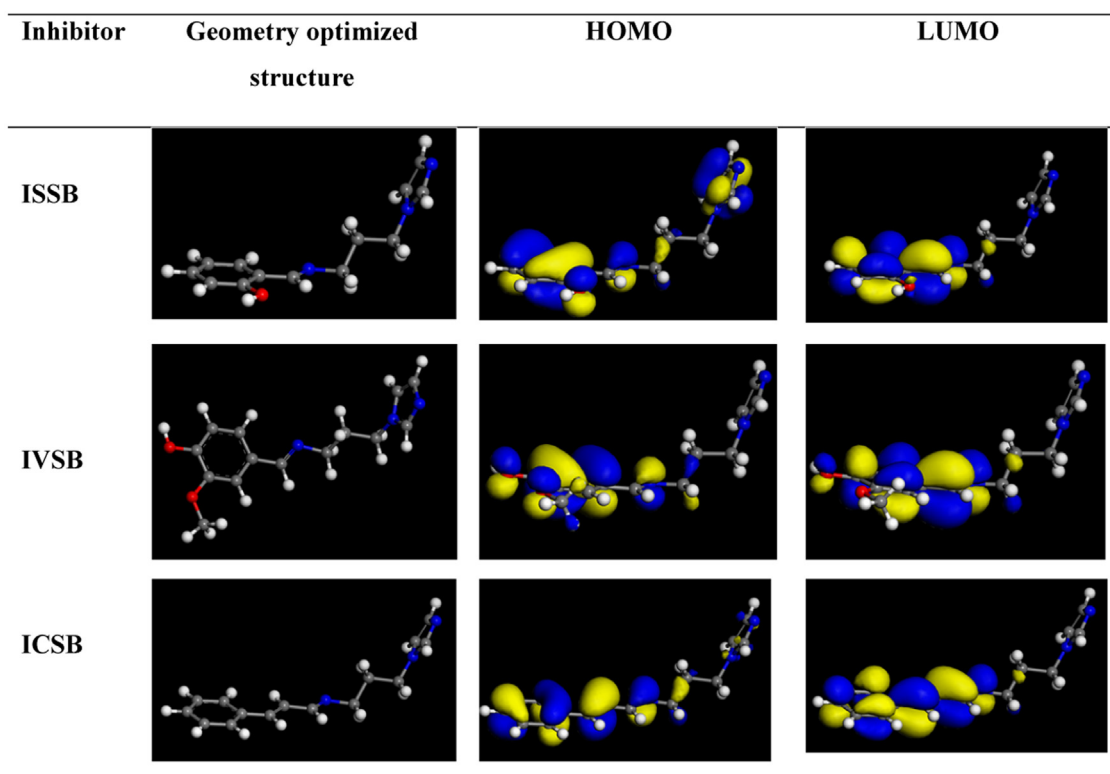
HOMO energy is seen to be the highest for IVSB and lowest for ISSB. Higher HOMO energy facilitates the electron transfer from inhibitor molecule to the metal. LUMO energy, on the other hand, is lowest for ICSB and highest for IVSB. Lower the energy of LUMO, higher will be easiness of retro electron transfer from the metal to the inhibitor molecule [67–69]. For adsorption of inhibitors on the metal surface and subsequent corrosion protection of the later, both the electron donation towards the metal and back electron transfer from the metal are important. Considering all these, it may be argued that lower energy gap between HOMO and LUMO is

Table 8
Elemental analysis of the surface by EDAX in the absence and presence of inhibitors.

Element	Weight % Polished surface	Uninhibited	ISSB	IVSB	ICSB
C	4.6	11.0	9.8	8.1	8.7
O		16.9	13.6	9.9	0.8
Si	1.3	0.8	0.8	0.6	0.9
S	0.5	0.7	0.5	0.5	0.4
Cl	0.3	0.8	0.9	0.5	0.2
Cr	0.3	0.4	0.4	0.3	0.3
Mn	0.5	0.5	0.4	0.6	0.7
Fe	92.4	68.8	73.0	79.2	87.9

Table 9
Molecular parameters of inhibitors calculated from DFT study (DND basis set).

Inhibitor	E_{HOMO} (eV)	E_{LUMO} (eV)	ΔE (eV)	χ (eV)	η (eV)	σ (eV ⁻¹)	ΔN_{110}
ISSB	-6.4023	-1.5309	4.8715	3.9666	2.4357	0.4106	0.1752
IVSB	-5.9868	-1.3279	4.6589	3.6574	2.3294	0.4293	0.2496
ICSB	-6.2765	-1.9016	4.37497	4.0890	2.1875	0.4572	0.1671

**Fig. 9.** Optimized geometry and electron distribution in HOMO and LUMO for three different imidazole-based Schiff bases as obtained from DFT study.

ideal for this conjugated effect of electron donation and acceptance [67–70]. Table 9 illustrates such correlation. ICSB exhibiting highest corrosion inhibition efficiency, has the smallest HOMO - LUMO energy gap, while ISSB being the least effective inhibitor among the three, possesses maximum energy gap between the frontier orbitals. Importance of back electron donation towards extent of interaction of inhibitor with the metal is also evident from the maximum value of electronegativity (χ) for ICSB. The two-way electron transfer is essential for any inhibitor to act as mixed type. When electron donation from the HOMO of inhibitor to the anodic sites on the metal surface happens, electron density in those sites increases, retarding the rate of metal dissolution reaction. Again, electron transfer from the cathodic sites on the metal to the in-

hibitor results into dearth of electron at those sites and consequently the rate of cathodic deposition current decreases. Thus, the experimentally observed mixed type inhibition property of the selected Schiff bases can be validated from theoretical consideration [3,8,9,71].

Global hardness and softness are two important parameters in regard to the molecular interaction. Lower hardness and higher softness are indicative towards better interaction of the inhibitor molecules with the metal surface [68–71]. Table 9 shows a perfect correlation among these parameters for the three inhibitors with their corrosion resistance effectiveness. The fraction of electron transferred from the inhibitor molecules to the (1 1 0) Fe plane is seen to be positive, which suggests the extent of forward

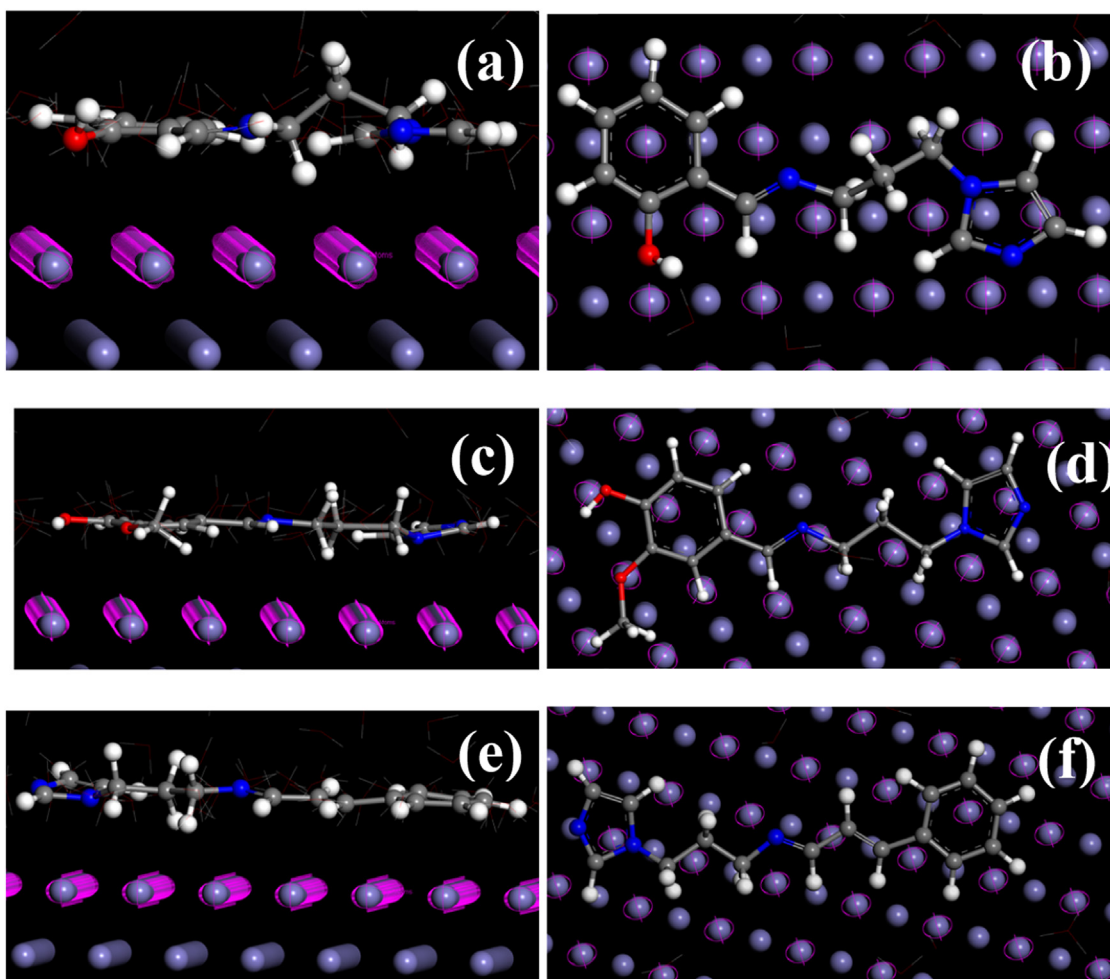


Fig. 10. Orientation of ISSB (a and b), IVSB (c and d) ICSB (e and f) on the Fe (1 1 0) surface as visualized from MD simulation (water molecules are not shown for clarity).

electron transfer from inhibitor to metal is more than the retro electron transfer. This value for ICSB is lower compared to others as the degree of back electron donation is maximum for ICSB due to its lowest LUMO energy level.

3.9. Fukui indices analysis

The atoms present in the inhibitor molecules, which are susceptible towards attack by a nucleophile and an electrophile are ascertained from the values of positive and negative Fukui indices, f_k^+ and f_k^- , respectively of the atoms. These values are shown in table S4 in SI. For ISSB, C and N atoms present in the imidazole moiety are active towards electron donation to the metal, as they possess higher values of f_k^- . C and O atoms present in the salicylaldehyde moiety along with the N of imine bond participate in bi-directional electron transfer (electron donation as well as acceptance) as they have high values of both the f_k^+ and f_k^- . High values of f_k^+ and f_k^- for C and O atoms of the vanillin moiety and N atom of the imine group present in IVSB suggest their involvement in the whole adsorption process through electron donation and acceptance. Similar inference can be drawn for the cinnamaldehyde moiety and the imine N present in case of ICSB.

3.10. MD simulation result

MD simulation outcomes which rely on the force-field modelled electrostatic interaction among the atoms present in inhibitor

Table 10

Interaction energy between inhibitor molecule and Fe (1 1 0) surface.

Inhibitor	Interaction energy (kcal/mol)
ISSB	-170.918
IVSB	-124.534
ICSB	-175.424

molecule and metal atoms in presence of the electrolytic solution are depicted in Fig. 10. It is observed that the electrostatic interaction forces the inhibitor molecules to adopt a planar configuration. Obviously, the molecules will be under some kind of stress. The interaction energy between the inhibitor molecules and the (1 1 0) Fe surface will depend on the extent of this stress. In general, more negative the interaction energy, higher will be the molecular interaction and hence the inhibition efficiency. ICSB exhibits maximum negative value and this is conducive for ICSB to impart maximum corrosion inhibition effect for mild steel in aqueous HCl (Table 10). For ISSB and IVSB, the order is interaction energy is in opposition to the experimentally observed inhibitory action (Table 10). This observation may be associated with inherent weakness of the MD simulation method. In the MD simulation, inhibitor/metal interaction is calculated based on the Van der Waals and electrostatic interactions, whereas the electronic aspect was not considered.

Additionally, in MD simulation we have to keep the Fe layers frozen. In fact, some recent studies suggest that the corrosion in-

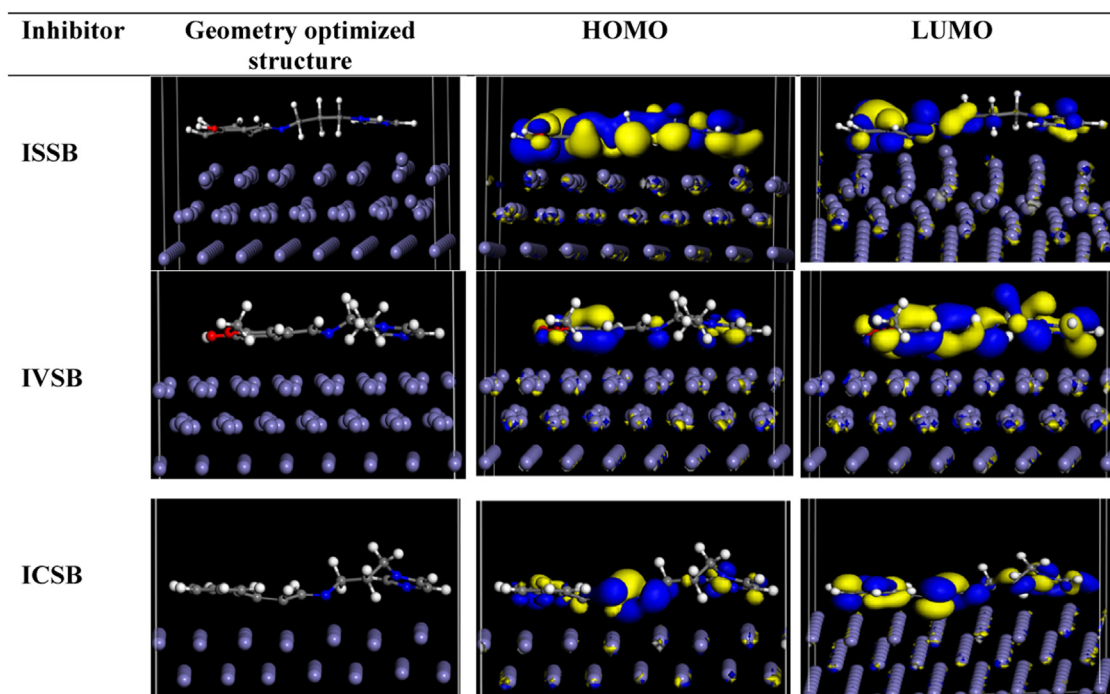


Fig. 11. Electron distribution in HOMO and LUMO for energy optimized inhibitor molecules obtained from DFTB+ study.

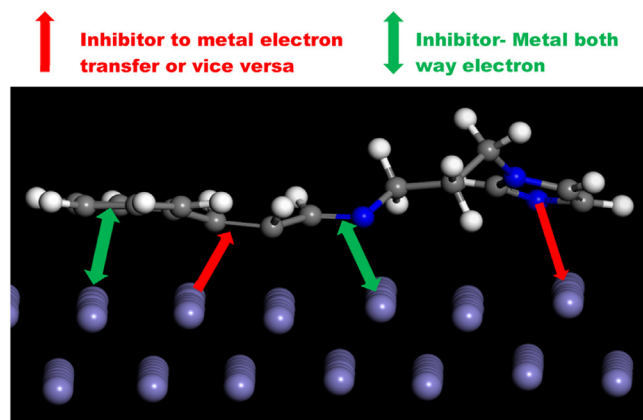


Fig. 12. Mode of adsorption of ICSB with metal surface following DFTB+ result.

hibitory property or the extent of molecular interaction, in general, cannot always be explained or predicted following DFT or MD calculations [27,31]. To overcome the limitations of this method, we have undertaken the Density Functional based Tight Binding (DFTB+) study.

3.11. DFTB+ study

In order to get more realistic interaction pattern between the Fe (1 1 0) surface atoms and inhibitor molecules, DFTB+ study using trans3d Slater-Koster library function (allows element interactions among Fe-C-H-N-O). The process is discussed in details in the Section 2.9. Fig. 11 shows the interaction pattern along with the electron distribution in HOMO and LUMO energy levels. Due to interaction, the distribution of Fe atoms in the upper two layers of (1 1 0) plane is severely ruptured. The Schiff bases assume almost flat orientation with respect to be Fe surface. This induces drastic changes in electron distribution in the frontier molecular orbitals compared to those in absence of the metal surface. For

Table 11

Interaction energy between inhibitor molecule and Fe slab (from DFTB+ study).

Inhibitor	Interaction energy (kcal mol ⁻¹)
ISSB	-814.9
IVSB	-944.8
ICSB	-1026.8

ISSB, HOMO is distributed over the whole molecular surface, while LUMO is distributed preferentially on the salicylaldehyde moiety together with the imine bond. For IVSB, HOMO is not evenly distributed over the whole surface, it encompasses the phenyl ring of vanillin moiety, N atom of imine bond and N atoms of imidazole group. LUMO on the other hand is all over the molecular surface. Similar behavior is seen for the LUMO of ICSB. HOMO in ICSB is mostly involved to the C=C and the attached C=N bonds in between the two aromatic groups. An atomistic approach towards mode of interaction of the inhibitor molecules with Fe surface can be extended by comparing the atomic charges before and after adsorption. In Fig. S10 in SI, the Mulliken charges of individual atoms before and after adsorption are shown. For unadsorbed ICSB, the charges on the C atoms of the phenyl ring of cinnamaldehyde moiety are in the range -0.070 – -0.087 . But when ICSB get adsorbed on Fe surface, these values change within a wide range of -0.136 – $+0.117$. This indicates that the phenyl group is involved for both way electron transfer with the Fe surface. When electron transfer happens from the inhibitor to the Fe surface, charges on the associated atoms become more positive, whereas on electron acceptance from the Fe surface these change towards more negative values. The charges of the C atoms present in C=C in conjugation with the phenyl group shift to more negative value when ICSB is adsorbed on the Fe surface (from -0.079 and -0.108 to -0.214 and -0.206). This also demonstrates involvement of retro-electron transfer from the Fe surface. Regarding the imidazole ring of ICSB, it is found that the charges on two C atoms and one N atom become more

Table 12
Inhibition efficiency along with structural features of some relevant Schiff bases.

Name/Schiff base derived from	Salient Structural feature	IE%	Ref.
Glycine + cinnamaldehyde	Cinnamaldehyde-amino acid conjugated Schiff bases having extended conjugation	96 at 1mM	3
Histidine + cinnamaldehyde		97 at 1mM	
Tryptophan + cinnamaldehyde		97.3 at 1mM	
Vanillin+ 2-(aminomethyl) Pyridine	Vanillin based Schiff base	87 at 1mM	8
Divanillin+ 2-(aminomethyl) Pyridine	Vanillin based double Schiff base	95 at 1mM	
4-phenoxyaniline + cinnamaldehyde	Additional –C=C– the bond between the imine group and aromatic ring extends the conjugation	94 at 0.1 mM	16
2-amino-5-mercapto-1,3,4-thiadiazole + cinnamaldehyde	Extended conjugation and also one thiol group	98 at 1mM	17
2-[2-(3-phenylallylidene)hydrazinecarbonothioyl)hydrazine carbonyl]benzoic acid	Extended conjugation and thiocarbonyl moiety	99 at 1.36 μM	18
Vanillin+2-cyanoguanidine	Vanillin based Schiff base	93 at 2.3 mM	74
Furoin thiosemicarbazone	Imine bond along with thiosemicarbazide moiety	98 at 2 mM	75
Salicylaldehyde chitosan Schiff base	Salicylaldehyde-biopolymer conjugated Schiff base	70 at 1500 ppm	76
Salicylaldehyde +semicarbazide	Second Schiff base has extended π-electron	79 at 0.5 mM	77
Salicylaldehyde + p-toluidine		86 at 0.5 mM	
N, N'- bis (salicylidene)-2-methoxyphenyl methanediamine	Double Schiff base with one additional –OCH ₃ substituent	97 at 1mM	78
N, N'- bis (salicylidene)-2- hydroxyphenyl methanediamine	Double Schiff base with one additional –OH substituent	96.5 at 1mM	
N, N'- bis (salicylidene)-phenyl methanediamine	Double Schiff base	89 at 1mM	
4-Aminoantipyrine+ p-hydroxybenzaldehyde	Benzaldehyde moiety contains substituents having different electron donating capacity	91.8 at 10mM	79
4-Aminoantipyrine+ p-methoxybenzaldehyde		91.6 at 10 mM	
4-Aminoantipyrine+ p-chlorobenzaldehyde		91.4 at 10mM	
4-Aminoantipyrine+ p-nitrobenzaldehyde		78 at 10mM	
4-Aminoantipyrine+ benzaldehyde		76.7 at 10mm	

positive upon adsorption. We thus may infer that imidazole ring of ICSB acts mostly as electron donor towards the Fe surface. For ISSB and IVSB, the phenyl group of the aldehyde part as well as the imidazole ring interact with the Fe surface in the similar way as those for ICSB. The O atoms present in the substituent groups of salicylaldehyde unit of ISSB and vanillin moiety of IVSB experience decrement in the negative charge upon adsorption. This validates the assumption of electron transfer from the heteroatom present in inhibitor molecule to the metal surface during adsorption. Interestingly, for all the three inhibitor molecules the charge on C and N atoms of the imine group do not change to any significant extent after adsorption. This indicates either non-involvement of the imine group or almost comparable extent of electron donation and acceptance by the imine group during adsorption. Based on these discussions most plausible mode of adsorption of ICSB with the metal surface is depicted in Fig. 12. The electron donation and acceptance processes are not identical for all the inhibitors. This has led towards variation of interaction energy of the inhibitors with metal surface. We can calculate the interaction energy following the similar equation as given in Section 2.8 (Eq. (10)). Relevant data is shown in Table 11.

The variation of interaction energy is in full confirmation with the corrosion inhibition propensity trend. Absolute values differ from those obtained in MD simulation method, as we could not consider the electrolytic solution while calculation. Thus DFTB+ which is a semi-empirical quantum mechanical method is a better alternative over the empirical MD method to predict the extent of interaction of a series of structurally comparable corrosion inhibitors with the metal surface. Bond distances between the heteroatoms and carbon atoms of the conjugated system present in inhibitor molecules with the Fe atoms are calculated (Fig. S11 in SI) and seen to be within a range of 2.2 Å to 2.7 Å. This ensures very close interaction which leads to chemisorption [72,73].

3.12. Comparative account with other relevant Schiff bases

Literature includes several reports with Schiff bases as corrosion inhibitor for mild steel in aqueous HCl. Some relevant works illustrating correspondence between structural features of Schiff bases with their anti-corrosion propensity towards mild steel in aqueous HCl at ambient temperature are summarized in Table 12.

Table reveals that the presence of electron donating substituents enhances the inhibitory performance of the Schiff bases [74–79]. A double Schiff base having two imine bonds are usually more active [8,78]. Extended aromatic π-electrons present in salicylaldehyde-p-toluidine conjugated Schiff base provides better inhibition effect over the hetero N atoms present in salicylaldehyde-semicarbazide conjugated Schiff base [77]. Extended conjugation imparts some positive impact towards inhibitory action [3]. Thiol group or C=S group along with extended conjugation is found to provide high inhibition efficiency [17,18]. But whether the effect is mainly due to the extended conjugation or the other heteroatoms present, particularly thiol or C=S group, cannot be ascertained unambiguously. This is because Schiff base having thiosemicarbazide moiety and without any extended conjugation is also seen to provide considerable amount of inhibition efficiency [73]. ICSB and IVSB as per the present work are more efficient over the other salicylaldehyde and vanillin based Schiff bases, respectively [8,72,76,77]. ICSB, in-spite-of not having any thiol or C=S group, is found to impart almost comparable inhibitory performance for those Schiff bases with extended conjugation [17,18]. This may be associated with a balance between hydrophilic and hydrophobic characteristics of the studied molecules. In addition, present study establishes that for structurally comparable molecules, incorporation of an additional –C=C– bond in-between the imine group and aromatic ring, which leads to extension of the conjugation, invokes better inhibitory performance over

the electron donating substituents. Precursors of all the three Schiff bases are easily available, relatively of low cost and a simple single step condensation reaction is enough for preparation of these inhibitors. Inhibitors are effective at very lower concentration level. All these factors ensure economic viability of the studied inhibitor molecules.

4. Conclusion

- Comparing corrosion inhibition potentiality of three different Schiff bases, ISSB, IVSB and ICSB, which are prepared through condensation between 1-(3-aminopropyl)imidazole and three naturally occurring aldehydes, namely salicylaldehyde, vanillin and cinnamaldehyde, respectively, ICSB behaves as superior inhibitor to restrict corrosion of mild steel in aqueous HCl. ICSB exerts 99% inhibition efficiency even after 48 h of exposure at 30 °C.
- Presence of an additional –C=C– bond in-between the imine group and aromatic ring, providing extended conjugation, leads to better corrosion inhibitory property over other structurally comparable Schiff bases having electron donating substituents.
- Inhibitors, particularly ICSB can withstand temperature as high as 60 °C with 96% inhibition efficiency for an exposure of 6 h in 1 M aqueous HCl.
- Layer of ICSB on mild steel surface exhibits irreversibility for some couple of hours in uninhibited 1 M aqueous HCl.
- The studied Schiff bases act as mixed type corrosion inhibitors and their adsorption property on mild steel surface is characterized as chemisorption involving partial displacement of pre-adsorbed water molecules.
- DFT and DFTB+ studies are instrumental to ascertain the mode of adsorption of inhibitors on metal surface through bi-directional electron transfer process.
- For ICSB, DFTB+ study reveals the C=C group of cinnamaldehyde moiety and the imine group are mostly responsible for electron donation to the metal surface, while the whole molecular surface is energetically conducive for retro electron transfer.
- Interaction energy calculated from DFTB+ study is seen to validate the corrosion inhibition trend of studied Schiff bases more accurately than those calculated through MD simulation method.

Declaration of Competing Interest

Authors declare no conflict of interest regarding the present work.

CRediT authorship contribution statement

Sanjoy Satpati: Conceptualization, Methodology, Investigation, Formal analysis. **Aditya Suhasaria:** Methodology, Investigation, Formal analysis. **Subhas Ghosal:** Software, Validation. **Utpal Adhikari:** Resources, Formal analysis, Funding acquisition. **Priyabrata Banerjee:** Resources, Funding acquisition. **Sukalpa Dey:** Visualization. **Dipankar Sukul:** Supervision, Funding acquisition, Writing – review & editing.

Data availability

All required data are available in the manuscript and supplementary file.

Acknowledgment

DS, AS thank Department of Science & Technology and Biotechnology, Government of West Bengal, India for supporting research

project no. 217(Sanc.)/ST/P/S&T/15G-10/2017 and providing a fellowship. UA and DS thank SERB, Government of India for providing computational facility through the project no. EMR/2017/005506. Infrastructural development of the Department of Chemistry, NIT Durgapur through DST-FIST grant of DST, Govt of India (no. SR/FST/CSI-267/2015) is also gratefully acknowledged.

Supplementary materials

Supplementary material associated with this article can be found, in the online version, at doi:10.1016/j.molstruc.2022.133684.

References

- [1] L. Ma, W. Li, S. Zhu, L. Wang, S. Guan, Corrosion inhibition of Schiff bases for Mg-Zn-Y-Nd alloy in normal saline: experimental and theoretical investigations, *Corros. Sci.* 184 (2021) 109268, doi:10.1016/j.corsci.2021.109268.
- [2] C. Verma, M.A. Quraishi, Recent progresses in Schiff bases as aqueous phase corrosion inhibitors: design and applications, *Coord. Chem. Rev.* 446 (2021) 214105, doi:10.1016/j.ccr.2021.214105.
- [3] S. Satpati, A. Suhasaria, S. Ghosal, A. Saha, S. Dey, D. Sukul, Amino acid and cinnamaldehyde conjugated Schiff bases as proficient corrosion inhibitors for mild steel in 1M HCl at higher temperature and prolonged exposure: detailed electrochemical, adsorption and theoretical study, *J. Mol. Liq.* 324 (2021) 115077, doi:10.1016/j.molliq.2020.115077.
- [4] L.O. Olasunkanmi, A.O. Idris, A.H. Adevole, O.O. Wahab, E.E. Ebenso, Adsorption and corrosion inhibition potentials of salicylaldehyde-based Schiff bases of semicarbazide and p-toluidine on mild steel in acidic medium: experimental and computational studies, *Surf. Interf.* 21 (2020) 100782, doi:10.1016/j.surfin.2020.100782.
- [5] S. Sengupta, M. Murmu, N.C. Murmu, P. Banerjee, Adsorption of redox-active Schiff bases and corrosion inhibiting property for mild steel in 1mol L⁻¹ H₂SO₄: experimental analysis supported by ab initio DFT, DFTB and molecular dynamics simulation approach, *J. Mol. Liq.* 326 (2021) 115215, doi:10.1016/j.molliq.2020.115215.
- [6] H. Keleş, M. Keleş, K. Sayin, Experimental and theoretical investigation of inhibition behavior of 2-((4-(dimethylamino)benzylidene)amino)benzenethiol for carbon steel in HCl solution, *Corros. Sci.* 184 (2021) 109376, doi:10.1016/j.corsci.2021.109376.
- [7] X. Lai, J. Hu, T. Ruan, J. Zhou, J. Qu, Chitosan derivative corrosion inhibitor for aluminum alloy in sodium chloride solution: a green organic/inorganic hybrid, *Carbohydr. Polym.* 265 (2021) 118074, doi:10.1016/j.carbpol.2021.118074.
- [8] S. Satpati, S.K. Saha, A. Suhasaria, P. Banerjee, D. Sukul, Adsorption and anti-corrosion characteristics of vanillin Schiff bases on mild steel in 1M HCl: experimental and theoretical study, *RSC Adv.* 10 (2020) 9258–9273, doi:10.1039/C9RA07982C.
- [9] A. Dutta, S.K. Saha, P. Banerjee, A.K. Patra, D. Sukul, Evaluating corrosion inhibition property of some Schiff bases for mild steel in 1M HCl: competitive effect of the heteroatom and stereochemical conformation of the molecule, *RSC Adv.* 6 (2016) 74833–74844, doi:10.1039/c6ra03521c.
- [10] W. Guo, M. Talha, Y. Lin, X. Kong, Schiff's base with center of symmetry as an effective corrosion inhibitor for mild steel in acid medium: electrochemical & simulation studies, *Colloids Surf. A Physicochem. Eng. Asp.* 615 (2021) 126234, doi:10.1016/j.colsurfa.2021.126234.
- [11] Y. Zhang, Y. Pan, P. Li, X. Zeng, B. Guo, J. Pan, L. Hou, X. Yin, Novel Schiff base-based cationic Gemini surfactants as corrosion inhibitors for Q235 carbon steel and printed circuit boards, *Colloids Surf. A Physicochem. Eng. Asp.* 623 (2021) 126717, doi:10.1016/j.colsurfa.2021.126717.
- [12] P. Shetty, Schiff bases: an overview of their corrosion inhibition activity in acid media against mild steel, *Chem. Eng. Commun.* 207 (2020) 985–1029, doi:10.1080/00986445.2019.1630387.
- [13] C. Verma, L.O. Olasunkanmi, E.E. Ebenso, M.A. Quraishi, Substituents effect on corrosion inhibition performance of organic compounds in aggressive ionic solutions: a review, *J. Mol. Liq.* 251 (2018) 100–118, doi:10.1016/j.molliq.2017.12.055.
- [14] S.M. Shaban, A.S. Salah, M. Tawfik, A. Abd-Elaal, I. Aiad, Corrosion inhibition and Biocidal effect of some cationic surfactants based on Schiff base, *J. Ind. Eng. Chem.* 19 (2013) 2004–2009, doi:10.1016/j.jiec.2013.03.013.
- [15] P. Visser, H. Terryn, J.M.C. Mol, On the importance of irreversibility of corrosion inhibitors for active coating protection of AA2024-T3, *Corros. Sci.* 140 (2018) 272–285, doi:10.1016/j.corsci.2018.05.037.
- [16] H. Keleş, M. Keleş, Electrochemical investigation of a schiff base synthesized by cinnamaldehyde as corrosion inhibitor on mild steel in acidic medium, *Res. Chem. Interf.* 40 (2014) 193–209.
- [17] R. Solmaz, Investigation of the inhibition effect of 5-((E)-4-phenylbuta-1,3-dienylideneamino)-1,3,4-thiadiazole-2-thiol Schiff base on mild steel corrosion in hydrochloric acid, *Corros. Sci.* 52 (2010) 3321–3330, doi:10.1016/j.corsci.2010.06.001.
- [18] I. Ahamad, C. Gupta, R. Prasad, M.A. Quraishi, An experimental and theoretical investigation of adsorption characteristics of a Schiff base compound as corrosion inhibitor at mild steel/hydrochloric acid interface, *J. Appl. Electrochem.* 40 (2010) 2171–2183.

- [19] D. Dwivedi, K. Lepková, T. Becker, Carbon steel corrosion: a review of key surface properties and characterization methods, *RSC Adv.* 7 (7) (2017) 4580–4610, doi:10.1039/C6RA25094G.
- [20] J.G. Speight, in: *Environmental Inorganic Chemistry For Engineers*, Elsevier, 2017, pp. 111–169, doi:10.1016/B978-0-12-849891-0.00003-5.
- [21] W. Gui, Y. Shi, J. Wei, Z. Zhang, P. Li, X. Xu, Y. Cuia, Y. Yang, Synthesis of N-(3-aminopropyl)imidazole-based poly(ionic liquid) as an adsorbent for the selective recovery of Au(III) ions from aqueous solutions, *New J. Chem.* 44 (2020) 20387–20395, doi:10.1039/D0NJ04420B.
- [22] R. Liu, Y. Dai, J. Li, X. Chen, C. Pan, J. Yang, Q. Li, 1-(3-Aminopropyl)imidazole functionalized poly(vinyl chloride) for high temperature proton exchange membrane fuel cell applications, *J. Membr. Sci.* 620 (2021) 118873, doi:10.1016/j.memsci.2020.118873.
- [23] A. Dutta, S.K. Saha, U. Adhikari, P. Banerjee, D. Sukul, Effect of substitution on corrosion inhibition properties of 2-(substitutedphenyl) benzimidazole derivatives on mild steel in 1M HCl solution: a combined experimental and theoretical approach, *Corros. Sci.* 123 (2017) 256–266, doi:10.1016/j.corsci.2017.04.017.
- [24] C. Verma, E.E. Ebenso, M.A. Quraishi, C.M. Hussain, Recent developments in sustainable corrosion inhibitors: design, performance and industrial scale applications, *Mater. Adv.* 2 (2021) 3806–3850, doi:10.1039/d0ma00681e.
- [25] A. Klamt, C. Moya, J. Palomar, A comprehensive comparison of the IEFPCM and SS(V)PE continuum solvation methods with the COSMO approach, *J. Chem. Theory Comput.* 11 (2015) 4220–4225, doi:10.1021/acs.jctc.5b00601.
- [26] E.E. Ebenso, C. Verma, L.O. Olasunkanmi, E.D. Akpan, D.K. Verma, H. Lgaz, L. Guo, S. Kaya, M.A. Quraishi, Molecular modelling of compounds used for corrosion inhibition studies: a review, *Phys. Chem. Chem. Phys.* 23 (2021) 19987, doi:10.1039/d1cp00244a.
- [27] A. Kokalj, M. Lozinšek, B. Kapun, P. Taheri, S. Neupane, P. Losada-Pérez, C. Xie, S. Stavber, D. Crespo, F.U. Renner, A. Mol, I. Milošev, Simplistic correlations between molecular electronic properties and inhibition efficiencies: do they really exist? *Corros. Sci.* 179 (2021) 108856, doi:10.1016/j.corsci.2020.108856.
- [28] R.G. Pearson, Absolute electronegativity and hardness: application to inorganic chemistry, *Inorg. Chem.* 27 (1988) 734–740, doi:10.1021/ic00277a030.
- [29] W. Yang, R.G. Parr, Hardness, softness, and the Fukui function in the electronic theory of metals and catalysis, *Proc. Natl. Acad. Sci. U.S.A.* 82 (1985) 6723–6726.
- [30] R.G. Pearson, Chemical hardness and density functional theory, *J. Chem. Sci.* 117 (2005) 369–377.
- [31] A. Kokalj, Molecular modeling of organic corrosion inhibitors: calculations, pitfalls, and conceptualization of molecule–surface bonding, *Corros. Sci.* (2021) 109650. doi:10.1016/j.corsci.2021.109650
- [32] A. Kokalj, On the HSAB based estimate of charge transfer between adsorbates and metal surfaces, *Chem. Phys.* 393 (2012) 1–12, doi:10.1016/j.chemphys.2011.10.021.
- [33] L. Guo, X. Ren, Y. Zhou, S. Xu, Y. Gong, S. Zhang, Theoretical evaluation of the corrosion inhibition performance of 1,3-thiazole and its amino derivatives, *Arab. J. Chem.* 10 (2017) 121–130, doi:10.1016/j.arabjc.2015.01.005.
- [34] P.K. Chattaraj, U. Sarkar, D.R. Roy, Electrophilicity Index, *Chem. Rev.* 106 (2006) 2065–2091, doi:10.1021/cr040109f.
- [35] B. Hourahine, B. Aradi, V. Blum, et al., DFTB+, a software package for efficient approximate density functional theory based atomistic simulations, *J. Chem. Phys.* 152 (2020) 124101, doi:10.1063/1.5143190.
- [36] F. Spiegelman, N. Tarrat, J. Cuny, L. Dontot, E. Posenitskiy, C. Martí, A. Simon, M. Rapacioli, Density-functional tight-binding: basic concepts and applications to molecules and clusters, *Adv. Phys. X* 5 (2020) 1710252, doi:10.1080/23746149.2019.1710252.
- [37] S. Choudhary, A. Garg, K. Mondal, Relation between open circuit potential and polarization resistance with rust and corrosion monitoring of mild steel, *J. Mater. Eng. Perform.* 25 (2016) 2969–2976, doi:10.1007/s11665-016-2112-6.
- [38] F.S. de Souza, A. Spinelli, Caffeic acid as a green corrosion inhibitor for mild steel, *Corros. Sci.* 51 (2009) 642–649, doi:10.1016/j.corsci.2008.12.013.
- [39] Ž.Z. Tasić, M.B.P. Mihajlović, M.B. Radovanović, A.T. Simonović, M.M. Antonijević, Cephadrine as corrosion inhibitor for copper in 0.9% NaCl solution, *J. Mol. Struct.* 1159 (2018) 46–54, doi:10.1016/j.molstruc.2018.01.031.
- [40] A. Suhasaria, M. Murmu, S. Satpati, P. Banerjee, D. Sukul, Bis-benzothiazoles as efficient corrosion inhibitors for mild steel in aqueous HCl: molecular structure-reactivity correlation study, *J. Mol. Liq.* 313 (2020) 113537, doi:10.1016/j.molliq.2020.113537.
- [41] A. Pal, C. Das, New eco-friendly anti-corrosion inhibitor of purple rice bran extract for boiler quality steel: experimental and theoretical investigations, *J. Mol. Struct.* 1251 (2022) 131988, doi:10.1016/j.molstruc.2021.131988.
- [42] R. Aydın, F. Köleli, Hydrogen evolution on conducting polymer electrodes in acidic media, *Prog. Org. Coat.* 56 (2006) 76–80, doi:10.1016/j.porgcoat.2006.02.004.
- [43] J.M. West, in: *Electrodeposition and Corrosion Processes*, D. Van Nostrand Co. Ltd., London, 1965, pp. 126–146.
- [44] B.N. Popov, in: *Corrosion Engineering: Principles and Solved Problems*, Elsevier, 2015, pp. 93–142.
- [45] T. Shinagawa, A.T. Garcia-Esparza, K. Takanabe, Insight on Tafel slopes from a microkinetic analysis of aqueous electrocatalysis for energy conversion, *Sci. Rep.* 5 (2015) 13801, doi:10.1038/srep13801.
- [46] A. Alobaid, C. Wang, R.A. Adomaitis, Mechanism and Kinetics of HER and OER on NiFe LDH Films in an Alkaline Electrolyte, *J. Electrochem. Soc.* 165 (2018) J3395–J3404.
- [47] F. Mansfeld, Electrochemical impedance spectroscopy (EIS) as a new tool for investigating methods of corrosion protection, *Electrochim. Acta* 35 (1990) 1533–1544, doi:10.1016/0013-4686(90)80007-b.
- [48] G.J. Brug, A.L.G. Van Den Eeden, M. Sluyters-Rehbach, J.H. Sluyters, The analysis of electrode impedances complicated by the presence of a constant phase element, *J. Electroanal. Chem.* 176 (1984) 275–295.
- [49] B. Hirschorn, M.E. Orazem, B. Tribollet, V. Vivier, I. Frateur, M. Musiani, Determination of effective capacitance and film thickness from constant-phase-element parameters, *Electrochim. Acta* 55 (2010) 6218–6227, doi:10.1016/j.electacta.2009.10.065.
- [50] P. Córdoba-Torres, T.J. Mesquita, O. Devos, B. Tribollet, V. Roche, R.P. Nogueira, On the intrinsic coupling between constant-phase element parameters α and Q in electrochemical impedance spectroscopy, *Electrochim. Acta* 72 (2012) 172–178, doi:10.1016/j.electacta.2012.04.020.
- [51] J.B. Jorcin, M.E. Orazem, N. Pébère, B. Tribollet, CPE analysis by local electrochemical impedance spectroscopy, *Electrochim. Acta* 51 (2006) 1473–1479, doi:10.1016/j.electacta.2005.02.128.
- [52] Z. Lukács, T. Kristóf, A generalized model of the equivalent circuits in the electrochemical impedance spectroscopy, *Electrochim. Acta* 363 (2020) 137199, doi:10.1016/j.electacta.2020.137199.
- [53] U. Rammelt, G. Reinhard, The influence of surface roughness on the impedance data for iron electrodes in acid solutions, *Corros. Sci.* 27 (1987) 373–382, doi:10.1016/0010-938X(87)90079-5.
- [54] A. Amirudin, D. Thierry, Application of electrochemical impedance spectroscopy to study the degradation of polymer-coated metals, *Prog. Org. Coat.* 26 (1995) 1–28, doi:10.1016/0300-9440(95)00581-1.
- [55] G.W. Walter, A review of impedance plot methods used for corrosion performance analysis of painted metals, *Corros. Sci.* 26 (1986) 681–703.
- [56] M. Meeusen, L. Zardet, A.M. Homborg, M. Lekka, F. Andreatta, L. Fedrizzi, B. Boelen, J.M.C. Mol, H. Terry, *Corros. Sci.* 173 (2020) 108780, doi:10.1016/j.corsci.2020.108780.
- [57] P. Kurzweil, Electrochemical energy storage for renewable sources and grid balancing, in: P.T. Moseley, J. Garche (Eds.), *Electrochemical Double-layer Capacitors*, Elsevier, 2015, pp. 345–407, doi:10.1016/B978-0-444-62616-5.00019-X.
- [58] E. McCafferty, N. Hackerman, Double layer capacitance of iron and corrosion inhibition with polymethylene diamines, *J. Electrochem. Soc.* (1972) 119–146.
- [59] K.F. Khaled, M.A. Amin, Corrosion monitoring of mild steel in sulphuric acid solutions in presence of some thiazole derivatives – Molecular dynamics, chemical and electrochemical studies, *Corros. Sci.* 51 (2009) 1964–1975, doi:10.1016/j.corsci.2009.05.023.
- [60] F. Mansfeld, T. Smith, E.P. Parry, Benzotriazole as corrosion inhibitor for copper, *Corrosion* 27 (1971) 289–294.
- [61] M. Finšgar, D.K. Merl, An electrochemical, long-term immersion, and XPS study of 2-mercaptobenzothiazole as a copper corrosion inhibitor in chloride solution, *Corros. Sci.* 83 (2014) 164–175, doi:10.1016/j.corsci.2014.02.016.
- [62] M.P. Hughes, K.D. Sensenthal, N.A. Ran, M. Seifrid, G.C. Bazan, T.Q. Nguyen, Determining the dielectric constants of organic photovoltaic materials using impedance spectroscopy, *Adv. Funct. Mater.* 28 (2018) 1801542, doi:10.1002/adfm.201801542.
- [63] M.S. Walczak, P. Morales-Gil, R. Lindsay, Determining Gibbs energies of adsorption from corrosion inhibition efficiencies: is it a reliable approach? *Corros. Sci.* 155 (2019) 182–185, doi:10.1016/j.corsci.2019.04.040.
- [64] X. Liu, X. Wang, F. Kapteijn, Water and metal–organic frameworks: from interaction toward utilization, *Chem. Rev.* 120 (2020) 8303–8377.
- [65] N. Kovac'ević, A. Kokalj, The relation between adsorption bonding and corrosion inhibition ofazole molecules on copper, *Corros. Sci.* 73 (2013) 7–17, doi:10.1016/j.corsci.2013.03.016.
- [66] N. Kovac'ević, A. Kokalj, Chemistry of the interaction between azole type corrosion inhibitor molecules and metal surfaces, *Mater. Chem. Phys.* 137 (2012) 331–339, doi:10.1016/j.matchemphys.2012.09.030.
- [67] J. Fang, J. Li, Quantum chemistry study on the relationship between molecular structure and corrosion inhibition efficiency of amides, *J. Mol. Struct. Theochem.* 593 (2002) 179–185.
- [68] Ş. Erdoğan, Z.S. Safi, S. Kaya, D.Ö. Işın, L. Guo, C. Kaya, A computational study on corrosion inhibition performances of novel quinoline derivatives against the corrosion of iron, *J. Mol. Struct.* 1134 (2017) 751–761, doi:10.1016/j.molstruc.2017.01.037.
- [69] A. Bouoidina, E. Ech-chihbi, F. El-Hajjaji, B. El Ibrahim, S. Kaya, M. Taleb, Anisole derivatives as sustainable-green inhibitors for mild steel corrosion in 1M HCl: DFT and molecular dynamic simulations approach, *J. Mol. Liq.* 324 (2021) 115088.
- [70] H. Bourzi, R. Oukhrib, B. El Ibrahim, H.A. Oualid, Y. Abdellaoui, B. Balkard, M. Hilali, S. El Issami, Understanding of anti-corrosive behavior of some tetrazole derivatives in acidic medium: adsorption on Cu (111) surface using quantum chemical calculations and Monte Carlo simulations, *Surf. Sci.* 702 (2020) 121692.
- [71] M. Mobin, R. Aslam, R. Salim, S. Kaya, An investigation on the synthesis, characterization and anti-corrosion properties of choline based ionic liquids as novel and environmentally friendly inhibitors for mild steel corrosion in 5% HCl, *J. Colloid Interface Sci.* 620 (2022) 293–312, doi:10.1016/j.jcis.2022.04.036.
- [72] Q.H. Zhang, B.S. Hou, Y.Y. Li, Y. Lei, X. Wang, H.F. Liu, G.A. Zhang, Two amino acid derivatives as high efficient green inhibitors for the corrosion of carbon steel in CO₂-saturated formation water, *Corros. Sci.* 189 (2021) 109596, doi:10.1016/j.corsci.2021.109596.

- [73] H. Lgaz, H. Lee, Facile preparation of new hydrazone compounds and their application for long-term corrosion inhibition of N80 steel in 15% HCl: an experimental study combined with DFTB calculations, *J. Mol. Liq.* (2021) 117952, doi:[10.1016/j.molliq.2021.117952](https://doi.org/10.1016/j.molliq.2021.117952).
- [74] C.M. Fernandes, V.G.S.S. Pina, C.G. Alfaro, et al., Innovative characterization of original green vanillin-derived Schiff bases as corrosion inhibitors by a synergic approach based on electrochemistry, microstructure, and computational analyses, *Colloids Surf. A Physicochem. Eng. Asp.* 641 (2022) 128540, doi:[10.1016/j.colsurfa.2022.128540](https://doi.org/10.1016/j.colsurfa.2022.128540).
- [75] K.S. Jacob, G. Parameswaran, Corrosion inhibition of mild steel in hydrochloric acid solution by Schiff base furoin thiosemicarbazone, *Corros. Sci.* 52 (2010) 224–228, doi:[10.1016/j.corsci.2009.09.007](https://doi.org/10.1016/j.corsci.2009.09.007).
- [76] R. Menaka, S. Subhashini, Chitosan Schiff base as eco-friendly inhibitor for mild steel corrosion in 1M HCl, *J. Adhes. Sci. Technol.* 30 (2016) 1622–1640, doi:[10.1080/01694243.2016.1156382](https://doi.org/10.1080/01694243.2016.1156382).
- [77] L.O. Olanokunmi, A.O. Idris, A.H. Adewole, O.O. Wahab, E.E. Ebenso, Adsorption and corrosion inhibition potentials of salicylaldehyde-based Schiff bases of semicarbazide and *p*-toluidine on mild steel in acidic medium: experimental and computational studies, *Surf. Interf.* 21 (2020) 100782, doi:[10.1016/j.surfin.2020.100782](https://doi.org/10.1016/j.surfin.2020.100782).
- [78] N. Soltani, M. Behpour, S.M. Ghoreishi, H. Naeimi, Corrosion inhibition of mild steel in hydrochloric acid solution by some double Schiff bases, *Corros. Sci.* 52 (2010) 1351–1361, doi:[10.1016/j.corsci.2009.11.045](https://doi.org/10.1016/j.corsci.2009.11.045).
- [79] A. Upadhyay, A.K. Purohit, G. Mahakur, S. Dash, P.K. Kar, Verification of corrosion inhibition of Mild steel by some 4-Aminoantipyrine-based Schiff bases – Impact of adsorbate substituent and cross-conjugation, *J. Mol. Liq.* 333 (2021) 115960, doi:[10.1016/j.molliq.2021.115960](https://doi.org/10.1016/j.molliq.2021.115960).